

國立臺灣大學理學院大氣科學所

碩士論文

Department of Atmospheric Sciences

College of Science

National Taiwan University

Master Thesis



以區域標記法進行閃電放電過程之模擬

Simulation of Lightning Discharge with Region-Labeling

Method

曾敏端

Min-Duan Tzeng

指導教授：陳正平 博士

Advisor : Jen-Ping Chen, Ph.D.

中華民國 107 年 7 月

July, 2018



## 國立臺灣大學碩士學位論文 口試委員會審定書

本論文係 曾敏端 君（學號 R05229008）在國立臺灣大學大氣科學學系、所完成之碩士學位論文，於民國 107 年 7 月 20 日承下列考試委員審查通過及口試及格，特此證明

口試委員：

陳正平

（簽名）

（指導教授）

周中富

楊明仁

陳昭志

系主任、所長

林+子雄

（簽名）

## 摘要



本研究利用天氣研究與預報模式(WRF)輔以大氣電學模組探討強降水與活躍閃電現象的關係。WRF 中的電學模組對於放電過程僅以基本圓柱狀結構描述，不能有效區分雲對地與雲內閃電放電過程。本研究改進放電通路的設定方式，以區域標記法對高電場區域進行連通，容許複雜幾何通路的放電計算，並且區分雲對地與雲內閃電，進一步對於不同放電特性進行計算。模擬結果顯示新方案能有效改進閃電放電頻率過高的現象，且閃電極性與雷暴雲微物理過程之間具有強烈關聯性:雲對地正閃電好發於軟雹初生的對流前期，雲內閃電好發於具有較強上升氣流的對流成熟期，雲對地負閃電則伴隨層狀區降水發生於對流消散期。以上閃電與對流結構發展的關聯性有助於強降水事件的即時預警。

關鍵字: 區域標記法、WRF 模式、閃電模擬、非感應電荷分離機制、總體參數法

## ABSTRACT



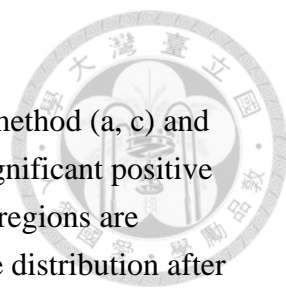
This study investigated the relationship between intense precipitation and vigorous lightning flashes using the Weather Research and Forecasting model coupled with an atmospheric electricity module WRF\_ELEC. The WRF\_ELEC module can describe basic discharging process, but it cannot identify intra-cloud and cloud-to-ground flashes. This study improved the discharging algorithm of WRF\_ELEC by applying the region-labeling method, which provides more detailed information on the electrical properties and geometry of lightning flashes. Simulation results show that the proposed method can significantly improve the lightning flash frequency. Also, it is able to reveal the polarity of lightning flash associated with the microphysical structure of thunderstorm. Positive cloud-to-ground flash is active at initial stage of thunderstorm when graupel formation becomes significant. Intra-cloud flash is active at the mature stage of thunderstorm when the updraft is strong enough to reach high levels. Negative cloud-to-ground flash is active during the dissipating stage of thunderstorm when precipitation results mainly from the outflow stratiform region. These important indicators are valuable for the nowcasting of heavy precipitation.

Keywords: Region-labeling method, WRF model, lightning simulation, non-inductive charge separation mechanism, bulk parameterization



## Table of Contents

1.	Introduction .....	1
2.	Methodology.....	5
2.1	Charging/Discharging Physics.....	5
2.2	Region-Labeling Method.....	10
2.3	Total Lightning Location System (TLDS).....	10
2.4	Model setup .....	11
3.	Results .....	13
3.1	Simulated convective system .....	13
3.2	Flash Frequency.....	14
3.3	Microphysics Structure.....	15
3.4	Charges in Hydrometeor.....	17
3.5	Polarity of Flash .....	19
3.6	Effective Channel Radii.....	20
4.	Summary and Future Work.....	21
	References .....	25
	Figures .....	29
	Table .....	44
	Appendix .....	45



## Index of Figures

Figure 2-1: A three-dimensional view of the discharge using the Cy method (a, c) and the RL method (b, d). Upper panels show the region with significant positive charges (orange) and negative charges (blue); the discharge regions are indicated with green-shading areas. Lower panels are charge distribution after flash. .... 29

Figure 2-2: The charge attached on graupel per-collision with ice/snow particle. The values below  $-40^{\circ}\text{C}$  are invalid and are filtered out during model iteration. *Mansell et al. (2005)* ..... 30

Figure 2-3: Schematic of the basic charge distribution in the convective region of thunderstorm. (*Stolzenburg et al. 1998*) ..... 30

Figure 2-4: The critical electric field for diagnosis of initial points of lightning. This is a demonstration of isothermal atmosphere with 293K. .... 31

Figure 2-5: A demonstration of RL method labels an individual channel. Blue grid is the initial grid with electric field magnitude greater than  $E_{init}$ . Gray grids are the grids with electric field greater than  $\tau E_{init}$ , which is the potential to join the channel. Red grids are grids which have been checked by RL method. Green grids are contiguous grids that join the channel. The algorithm terminates while all of the grids in the channel have been checked by RL method. .... 32

Figure 2-6: Domain configuration of the WRF model. Black block region is the nested second domain with 4 km grid spacing. Red block is the nested third domain with  $4/3$  km grid spacing. .... 33

Figure 2-7: Synoptic weather chart at initial time of simulation, 1800 UTC, May 24<sup>th</sup>, 2008 ..... 33

Figure 3-1: Frequency of independent cloud series lifetime. .... 34

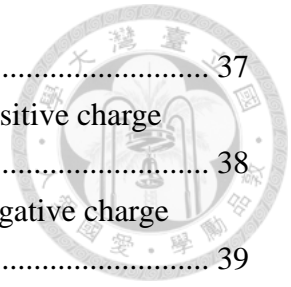
Figure 3-2: Evolution of the main cloud series. Each dot is a contiguous cloud segment. Colors denote the volume ratio of upward motion of each cloud segment. .... 34

Figure 3-3: Time series of IC (a) and CG (b) frequency, and flashes overlapped with domain-averaged precipitation (c). The total number of flashes through the entire simulation is noted at legend. Note that Cy only simulate total flashes which makes no difference between IC and CG. The scales of RL and observed flashes are shown on the left axis, whereas that of Cy is shown on the right axis. The time axis of observation is shifted and labeled at the upper axis. .... 35

Figure 3-4: Evolution of the vertical profile of hydrometeor contents in one of the largest thunderstorm cell. The cell is determined by 0.1 g/kg condensed phase water contiguous region with similar RL approach. QI: cloud ice; QS: snow; QG: graupel; QC: cloud drop; QR: rain drop ..... 36

Figure 3-5: Similar to Figure 3-4, excepts it shows the tendency of hydrometeor

contents.....	37
Figure 3-6: Similar to Figure 3-4, excepts it shows the cumulative positive charge attached on hydrometeors.....	38
Figure 3-7: Similar to Figure 3-4, excepts it shows the cumulative negative charge attached on hydrometeors.....	39
Figure 3-8: Similar to Figure 3-4, excepts it shows the average space charge density. Top: customized colorbar for positive charges; bottom: customized colorbar for negative charges. ....	40
Figure 3-9: Proportion of charges carried by hydrometeors in three types of flashes. Left panels (a, c, e) are the limiting reagent of lighting: positive charges for PCG (a), negative charges for NCG (c) and minor charges for IC (e). Right panels (b, d, f) are opposite-sign charges. Horizontal axis is the electric quantity of the limiting reagent which determines the magnitude of neutralization. ....	41
Figure 3-10: Frequency of effective channel radii under different insulating factor scenario.....	42
Figure 3-11: Relation between effective channel radii and quantity of electric charge inside channel. Shading denotes the CG counts. Contour denotes the IC counts with values of 1, 10, 100, 1000. ....	43



## Index of Table

Table 1: Notable option of the WRF model as used used this study. .... 44








## 1. Introduction

Lightning occurs extensively in severe weather and can inflict casualties and economic loss. The victims struck by lightning have 10-30% death rate, and most of the survivors suffered from permanently disabled body functions (*Ritenour et al.* 2008).

Lightning flash also creates electromagnetic pulses which can disrupt or damage electronic components. The mechanism of lightning and the relationship between flashes and heavy precipitation have interested researchers for decades. From the aspect of long-term climatology, lightning plays an important role on the formation of  $\text{NO}_x$  and  $\text{O}_3$ , which are important troposphere greenhouse gases, during summertime (*Zhang et al.* 2003). In addition, the polarized ice crystals that orientate along the electric field affect the albedo of anvil significantly. From the aspect of weather forecast and nowcast, the thunderclouds with more flashes indicate that their ice phase process is more active, subsequently producing heavier precipitation and, in extreme cases, resulting in destructive hailstones. On the microscopic scale, charged hydrometeors may have higher accretion rate and retain large sizes without breakup during collision. Therefore, understanding the formation of lightning in thunderstorm is valuable for risk assessment and for studying feedbacks of atmospheric electricity.

Lightning discharge is a rapid adjustment process that releases the instability in



atmospheric electrical field. This process is difficult to simulate with weather models (e.g. the Weather Research and Forecasting (WRF) model) due to the extraordinary scale variation of discharging channels. The width of lighting channel (around an inch) is much smaller than the grid size (0.5~30 km) of weather system models. On the other hand, the length of lightning branches can stretch over numerous grids; therefore, cross-grid communication is essential for lightning scheme. As such, current numerical algorithm of discharge scheme depends on the spatial and temporal scale of the model. Moreover, the time step used in the mesoscale model is much larger than that of the lightning flash, so the whole cycle of discharge needs to be resolved instantaneously.

Lightning simulation methods can be divided roughly into two approaches: explicit channels flash and bulk flash. One example of explicit channels flash is the dielectric breakdown model (*Niemeyer et al.* 1984, *Wiesmann and Zeller* 1986, *Mansell et al.* 2002), which is originally applied to the breakdown process of plastics or gases. This sort of model simulates step-by-step propagation of channel extension and branching. Branching, bonding or extension of channel relates to the ambient electric field as a probability function for any new segment that joins the channels. Each propagation step iterates the electric potential to make sure that the channels are equipotential. The simulation results are similar to the dielectric breakdown experiments. The channels tend to propagate and branch in the region of larger charge density. However, the scale

of dielectric breakdown models is much smaller than typical time steps and thus not practical to be use in the WRF model.



The bulk lightning scheme reduces the sophistication of lightning structure by using simple channel shapes. The parameterization in *Helsdon et al.* (1992) is a simple rod that traces the environmental electric field bi-directionally, and can only perform inter-cloud or intra-cloud (IC) channeling. The branching phenomenon is suppressed because of the geometry limitation. *MacGorman et al.* (2001) presented a revised lightning parameterization with a dumbbell shape to simulate the branched region with high charge density at both ends of bidirectional channels. Since the space charge is usually lifted in the air, cloud-to-ground (CG) channels are diagnosed from the channel with low base. To simplify the lightning process and adapt to the WRF model, *Fierro et al.* (2013) parameterized the channels using a cylindrical-shape discharging zone around the initiation points. The channels stretch from ground to the top of model, such that all channels are CG channels. In contrast to previous bulk lightning schemes, this study incorporated the region-labeling (RL) method, which was commonly used in image processing and also applied in convective cell analysis (*Tsai and Wu 2017*), to allow for more flexible geometry of lightning discharging regions, and also to differentiate between IC and polarized CG.

The main objectives of this study are to better understand how the geometry of

discharging channel affects the lightning flashes properties, and to investigate the possibility of nowcasting heavy precipitation using lightning signal.



## 2. Methodology



This study used the three-dimensional compressible nonhydrostatic WRF model (version 3.7.1) with Advanced Research WRF dynamic solver (WRF-ARW; Skamarock *et al.* 2008). The initial and atmospheric electricity variables are derived by additional physics module WRF\_ELEC (Fierro *et al.* 2013) that is specifically incorporated into the National Severe Storms Laboratory (NSSL) two-moment four-ice microphysics scheme, which applies the charging physics from Mansell *et al.* (2005). The main improvement in this study is the identification of lightning discharge channels. Basic lightning discharge channel in WRF\_ELEC assumes cylindrical geometry centered at lightning initiation points. The proposed discharging method adapts the RL algorithm (Tsai and Wu 2017) for both IC and CG identifications with flexible shapes related to ambient electric field. The geometry difference of the above method is illustrated in Fig. 2-1. A thunderstorm case in 2008 over northern Taiwan is selected for model simulation.

### 2.1 Charging/Discharging Physics

#### 2.1.1 Charging mechanism

A series of laboratory experiments (Takahashi 1978, Gardiner *et al.* 1985, Jayaratne *et al.* 1983, Ziegler *et al.* 1991, Brooks *et al.* 1997, Saunders and Peck 1998) suggested that non-inductive charge separation from riming graupel colliding with other solid



hydrometers plays a big role in thunderstorm electric field construction. Laboratory experiments generally agreed that the charges attached on graupel by non-inductive charge separation are positive sign under high temperature and high riming accretion rate (RAR) as illustrated in Fig. 2-2. This study calculates the non-inductive charge for grid cell with the following equation (*Mansell et al.* 2005):

$$\delta q = BD_f^a (V_g - V_I)^b q(RAR) \quad (1)$$

where  $B$ ,  $a$ ,  $b$  are coefficients depending on crystal size (cf. Table 1 in *Mansell et al.* 2005); subscript g and I represent graupel and the other ice-phase hydrometeor;  $D$  is the mean volume diameter;  $V$  is mass-weighted terminal fall speeds;  $q(RAR)$  is charge separation factor given by *Mansell et al.* (2005):

$$q_+(RAR) = 6.74(RAR - RAR_c) \quad (2a)$$

for positive charging ( $RAR > RAR_c$ ),

$$q_+(RAR) = 3.9(RAR_c - 0.1) \times \left( 4 \left[ \frac{RAR - (RAR_c - 0.1)/2}{RAR_c - 0.1} \right]^2 - 1 \right) \quad (2b)$$

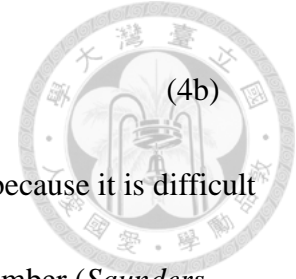
for negative charging ( $0.1 \text{ gm}^{-2} \text{ s}^{-1} < RAR < RAR_c$ ).

The critical RAR ( $RAR_c$ ) is given by Eqs. (21-23) in *Mansell et al.* (2005):

$$RAR_c(T) = \begin{cases} s(T): & T > -23.7^\circ\text{C} \\ k(T): & -23.7^\circ\text{C} > T > -40^\circ\text{C} \\ 0 : & T \leq -40^\circ\text{C} \end{cases} \quad (3)$$

$$s(T) = 1 + 7.9262 \times 10^{-2}T + 4.4847 \times 10^{-2}T^2 + 7.4754 \times 10^{-3}T^3 + 5.4686 \times 10^{-4}T^4 + 1.6737 \times 10^{-5}T^5 + 1.7613 \times 10^{-7}T^6 \quad (4a)$$

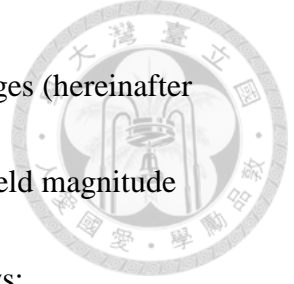
$$k(T) = 3.4 \left[ 1 - \left( \frac{|T+23.7|}{-23.7+40} \right)^3 \right] \quad (4b)$$



However, the  $RAR_c$  for the charging-sign reverse is still uncertain because it is difficult to control the surface property of mixture hydrometeors in cloud chamber (*Saunders* 2008). The charge separation may come from the mass transfer of quasi-liquid layers of hydrometeors (*Baker et al.* 1994). Because of the polarity of water, an overall electrically neutral hydrometeor tends to be negative at the surface and positive in its core. The negative charges at the surface transfer to another hydrometeor following the mass flow of quasi-liquid layers when collision happens. Mass flow direction depends on the thickness difference of quasi-liquid layers between hydrometeors. Hydrometeors with warmer surface or higher growth rate have thicker quasi-liquid layers, and may lose its mass when collision happens. Therefore, one hydrometeor, which has thicker quasi-liquid layer, is positively charged after collision, and the other one is negatively charged. Prior studies (*Krehbiel* 1986, *Stolzenburg et al.* 1998) show that there are two mainly charged region at middle and upper level of thunderstorms. The middle one is negatively charge and the other is positively charged (Fig. 2-3). There are thin charged layers of opposite sign at the boundary of cloud base (positive) and cloud top (negative), which are the inductive charges caused by main charged region.

### 2.1.2 Discharging Mechanism

The original WRF\_ELEC uses a cylindrical volume with prescribed radius



(typically 12 km) around the initial points to redistribute spatial charges (hereinafter called the Cy method). The initial points are the grids with electric field magnitude greater than an altitude-dependent threshold,  $E_{init}$ , defined as follows:

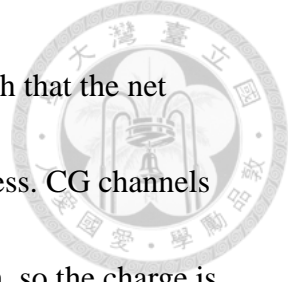
$$E_{init} = 2.84 \times 10^2 \left( \frac{kV}{m} \right) \frac{\rho}{\rho_0} \quad (5)$$

$$E_{init} \in (50, 180) \frac{kV}{m}$$

where  $\rho$  is the density of air and  $\rho_0=1.225 \text{ kg/m}^3$  is a constant. Values of  $E_{init}$  from the above equation is illustrated in Fig. 2-4. The channel size of the Cy method is specific and does not depend on the ambient electric field. All spatial charges inside the volume participate in the discharge. Neutralization of charges depends on the total amount of charges (positive or negative) inside the channel and the charge density. Charge density structure is conserved inside the channel but with a smaller magnitude because of the neutralization of charges. However, there is no difference between the neutralization of charges of IC and CG flashes.

This study modified the discharge module by determining the channel with RL method (details given in the next section). The RL method connects adjacent regions with significant electric field. The critical electric field is set to be a portion of  $E_{init}$  using an insulating factor,  $\tau$ . Grids with electrical field magnitudes greater than  $\tau E_{init}$  can then join the lightning flash channels. This method automatically changes the geometry of channel according to the ambient electric field. IC and CG are identified





through the altitude of channel base. IC channels occur in the air, such that the net charge in the atmosphere is conserved during the neutralization process. CG channels connect to the ground and direct the atmospheric charges to the Earth, so the charge is not conserved in the air. The equations of charge neutralization are expressed as follows:

$$PCG : dq = \begin{cases} -\gamma q & q > 0 \\ -\gamma q \frac{P}{N} & q < 0 \end{cases} \quad (6a)$$

$$NCG : dq = \begin{cases} -\gamma q \frac{N}{P} & q > 0 \\ -\gamma q & q < 0 \end{cases} \quad (6b)$$

$$IC : dq = \gamma(\bar{q} - q) \quad (6c)$$

where *PCG* and *NCG* indicate positive and negative CG, respectively;  $q$  is the charge density and  $dq$  is the change in charge density due to neutralization;  $\bar{q}$  is the average charge density in the channel;  $N$  and  $P$  are total negative and positive charges in the channel, respectively; and  $\gamma$  is a prescribed coefficient to control the magnitude of neutralization. Magnitude of grounding current in CG depends on the major sign charge in the channel. On the other hand, neutralization of charge in IC is limited by the minor sign charge in the channel. Charges remaining from neutralization are redistributed according to the charge density before discharge. To compare with the Cy method, the effective radius of channel is defined as follows:

$$R_{ch} = \sqrt{\frac{V_{ch}}{\pi D_{ch}}} \quad (7)$$

where  $R, V, D$  are radius, volume and depth of channel, respectively.

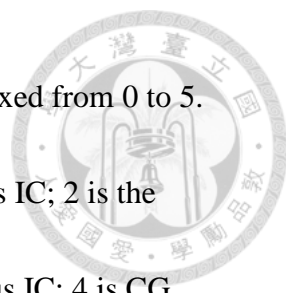


## 2.2 Region-Labeling Method

The region-labeling (RL) method (also called connected-component labeling or blob extraction) is an algorithm commonly used in computer visualization (*Ballard and Brown 1982*) and has also been applied in cloud object analysis (*Heiblum et al. 2016; Tsai and Wu 2017*). The algorithm detects contiguous region with a key property above a prescribe threshold, as demonstrated in Fig. 2-5. In this study, the concerned property is the electric field magnitude. The RL method is also applied to track convective cells in this study (with the concerned property of cloud condensate amount). The temporal tracking targets a series of convective cells by the overlapping region in the continuous time interval, which is 2 minutes in this study.

## 2.3 Total Lightning Location System (TLDS)

The lightning data used in this study were from the Total Lightning Location System (TLDS) measurements provided by the Taiwan Power Company. The TLDS is an array of antenna that detects and ranges lightning by measuring the arrival time of LF/HF radiation from CG flashes at multiple stations. For IC events, TLDS measures the interferometry of VHF radiation and reports the two-dimensional location of flashes projected on the ground. The system is more sensitive to IC than to CG events because of the limitation of frequency band.



The TLDS divides the lightning impulses into six categories indexed from 0 to 5. Category 0 is singleton IC signal; 1 is the initial signal for continuous IC; 2 is the transitional signal of continuous IC; 3 is the termination of continuous IC; 4 is CG signal; 5 is returning stroke of CG. The simulated lightning is compared with category 0 for IC and category 4 for CG, and the polarity of CG is determined by the sign of peak current.

## 2.4 Model setup

The domain configuration and some notable options selected in WRF model are shown in Fig. 2-6 and Table 1. The model runs with Cy lightning discharge method and the RL method mechanism are designated as the control and experiment runs, respectively. The insulating factor  $\tau$  is set to 0.2 for the main simulation. The sensitivity of  $\tau$  is evaluated by virtual lightning discharge, and does not affect the electricity of main simulation, with  $\tau$  ranged from 0.2 to 0.8.

Figure 2-7 shows the synoptic weather chart at the initial time of simulation, which is 18:00 UTC, May 24<sup>th</sup>, 2008. The unstable weather condition before the mei-yu front arrival is favored for thunderstorm activities. The convection system in the simulation is quasi-stationary at the offshore region and over the terrain. The rationale behind the case selection is that RL method is a serial algorithm that cannot afford a large domain

for fast convective system propagation.



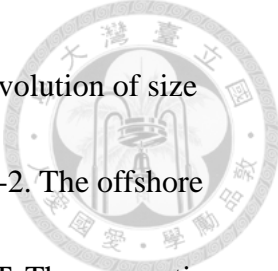


### 3. Results

#### 3.1 Simulated convective system

Appendix A1 shows the composite reflectivity from the Central Weather Bureau (CWB) radars and simulated by model from 06:00 to 22:00 LST, May 25<sup>th</sup>, 2008. Note that the simulated electricity does not feedback to the microphysics or environmental properties, therefore both RL and Cy methods have identical precipitation and storm microphysical structures. There are two major convective systems in the simulation. The earlier convective system was initiated at an offshore region, and is weaker than the later one. The convective system simulated is somewhat stronger than observed, and is more aggregated which exhibited a more linear structure. The later convective system was initiated over land and propagated westward to merge with the dissipating offshore convective system. By looking at the composite radar reflectivity and time series of lightning flashes, it is found that the simulated systems lead the observed systems. So, the simulated results are shifted forward by 3 hours in the comparison analyses.

With output rate of every two minutes, there are 121044 cloud segments being labeled in this one-day simulation. Among the 121044 cloud segments, there are 7073 cloud series with their life-time distribution shown in Fig. 3-1. The lightning flashes are produced by only one of the cloud series, which is the major series with 77504 segments including those being merged or split up. This series contains two major




convective systems, one offshore and the other over the terrain. The evolution of size and the ratio of updraft (speed  $> 0 \text{ m s}^{-1}$ ) volumes are shown in Fig. 3-2. The offshore convection was initiated at 06:20 LST and diminished after 10:30 LST. The convective system over terrain was initiated as chaotic convective cells from 09:20 to 11:40 LST and then organized into a large convective system. A significant merger event seemed to happen at 19:00; however, it is actually a merger between two dissipating anvil, which marked the decline of the convection system that contrasts with the organization of the chaotic convections. The following discussion of microphysical and electrical properties is focused on this major cloud series.

### 3.2 Flash Frequency

The simulated frequencies of IC (Fig. 3-3a) and CG (Fig. 3-3b) flashes are of a similar magnitude as observed, except during the peak hours of 13:00 to 15:00 LST when the model underestimates IC and overestimates CG counts. However, the total flash counts are similar. These biases are caused by the low  $\tau$  value that used which tends to connect channel to ground. Thus, the CG channels release more energy than usual and suppress the IC channels. In comparison, the Cy method generally overestimates the total flash counts by a factor of two.

Figure 3-3c shows that PCG peak occurred at the early stage of thunderstorm

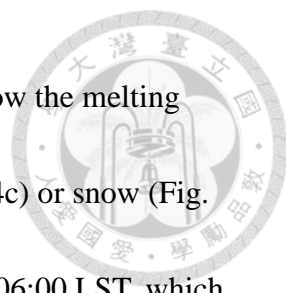


activity, and it leads the precipitation peak by about an hour, which is different from the results of *Tai et al.* (2017), who found that IC peak leads precipitation. IC flashes developed following PCG during the mature stage of thunderstorm but without a significant peak. NCG developed even later, with two major peaks occurred during the dissipation stage of thunderstorm. After the second NCG peak, the precipitation terminated as the storms die out.

The PCG flashes concentrated at the updraft region while the IC flashes are around the edges of the updraft region (Appendix A2). On the other hand, the NCG flashes distributed sporadically at the outflow stratiform region of the convection (Appendix A3). The polarity of RL CG is opposite to the TLDS observed. The uncertainty of lightning polarity and the relationship between precipitation and flashes will be discussed in Section 3.3 and 3.4.

### **3.3 Microphysics Structure**

Figure 3-4 shows the water content (mixing ratio) and tendency (Fig. 3-5) of each hydrometeor category (QC: cloud drop; QR: raindrop; QI: cloud ice; QS: snow; and QG graupel) in the main cloud system. The earlier convection offshore produces less precipitation than the subsequent convection over terrain that developed after 09:20 LST. At the initial stage of both convections, particles in cloud are mainly cloud drops (Fig.



3-4d) and cloud ice (Fig. 3-4a). Raindrops (Fig. 3-4e) developed below the melting level, indicating that they should be originated from graupel (Fig. 3-4c) or snow (Fig. 3-4b) melting. Significant riming for graupel formation happened at 06:00 LST, which is also the time for the first (but minor) PCG peak. Explosive formation of graupel happened around 11:00 LST when the second and major peak of PCG occurred. The upward-tilting-with-time pattern in cloud drops (Fig. 3-5d) and cloud ice (Fig. 3-5a) suggests that these two hydrometeors form at the lifting region. In contrast, some downward propagating patterns happen in raindrops (Fig. 3-5e) and snow (Fig. 3-5b) because these two hydrometeors grow by accreting other hydrometeors while falling. The high variability of cloud drops tendency indicates that cloud drops form in the convective region with significant updraft and downdraft. On the other hand, cloud ice tendency is smoother than that of cloud drop because it mainly forms at the stratiform region of cloud. The patterns of convective and stratiform regions can also be found in the tendency of raindrops and snow, respectively. The graupel tendency (Fig. 3-5c) has no significant vertical-propagation pattern, because the tendency of graupel depends on the cloud drop concentration and the rimed ice/graupel particle size. The concentration of cloud drop is greater at lower levels, but the rimed particles are somewhat higher levels. Thus, the tendency of graupel is vertically invariant.

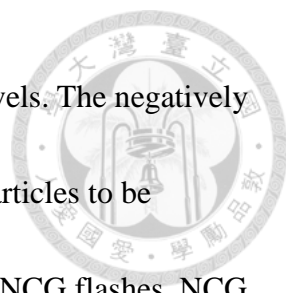




### 3.4 Charges in Hydrometeor

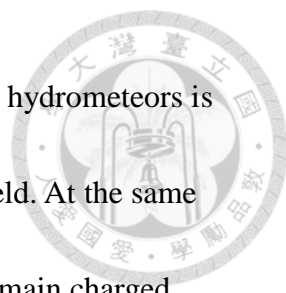
Figures 3-6 and 3-7 show the charges carried by graupel, cloud ice, snow and rain drops. Graupel particles that collide with ice particles tend to carry positive charges at low (warmer) altitudes (Fig. 3-6a) and negative charges at high (cooler) altitudes (Fig. 3-7a), as the process depends on the ambient temperature and riming rate (Fig. 2-2). Ice particles that collide with riming graupel at lower levels carry negative charges to the higher levels and reach to the top of thunderstorm. These negatively charged ice particles aggregate with each other and form snow particles, which combine the negative charges from the colliding particles (Fig. 3-7b). On the other hand, ice particles that collide with riming graupel at higher levels tend to carry positive charge. These positively charged ice particles can aggregate and form positively charged snow particles (Fig. 3-6b) at the middle level.

PCG peak revealed significant riming process at low levels. Graupel particles grew explosively by riming process and produced plenty of positively charged graupel particles that fall toward the cloud base. The concentrated charges at the cloud base induced significant PCG flash events before heavy precipitation arrived at the ground. Unceasing IC indicates that the updraft is strong enough to produce large snow particles which carried negative charges. The negatively charged snow particles fall to lower levels and neutralized the air containing positively charged graupel particles.



NCG peak is the signal of termination of electrification at low levels. The negatively charged particles fall to cloud base without any positively charged particles to be neutralized. Therefore, negative charges released to the ground form NCG flashes. NCG flashes also occurred in the outflow stratiform region of convective cloud, therefore the electrification at low level is weak.

Figure 3-8 shows the space charge density in the cloud. The thunderstorm is overall negatively charged. These are the remaining charges from the active PCG. Although the size of lower positive region seems to be large as shown in Appendix A3, the charge density is much less than the negative charge at middle level (Fig. 3-8). The top positively charged region is also insignificant and somewhat overwhelmed by negative charges. The graupel particle at low altitude carries more positive charges than conventional knowledge, and ice particle carrying negative charge also contrasts with prior studies (*Krehbiel 1986, Stolzenburg et al. 1998*). According to the conventional knowledge of thunderstorm with triple-pole structure (main negative, upper and lower positive charged region; Fig. 2-3), the riming accretion rate in thunderstorm should lower than  $1 \text{ gm}^{-2}\text{s}^{-1}$  (Fig. 2-2), as such the main charge region at lower level is negatively charged and the upper level is positively charged. These results indicate that the charging mechanism (Fig. 2-2) in the model may have some bias or the simulated riming rates are unrealistically large, which lead to positive charging of graupel at low



level. If an additional description of electric polarization of dielectric hydrometeors is added into the model, this could reduce the instability of electrical field. At the same time, it would induce opposite charge layers at the boundaries of the main charged regions. These layers would reduce the cloud-to-ground flashes at cloud base and trigger the transient luminous events at cloud top. Although this research focused on the discharging process, it is nonetheless important to re-examine the charging mechanism and the effects of dielectric property of hydrometeors in the future.

### **3.5 Polarity of Flash**

Figure 3-9 shows the proportion of positive and negative charges carried by hydrometeors in three types of flashes (i.e., PCG, NCG and IC). As indicated by Eq. (6), the limiting reagent of charge neutralization is the positive charges, negative charges and minor sign charges for PCG, NCG and IC, respectively. The results here agree with the hypothesis discussed in the previous section. The most important electrified hydrometeor is graupel, which carried about 80% of positive charges in PCG (Fig. 3-9a). For the negative-charge-major IC (positive part of Fig. 3-9e), graupel particles also carry 80% of positive charges in the channel. These two types of flash are the most frequent flashes in simulated thunderstorms. For NCG at the dissipating stage of storm activity, 50% of negative charges are on cloud ice while 40% are on snow. This strongly

suggests that PCG and IC are indicators for the intense formation of low level graupel particles which is a prerequisite for heavy precipitation formation.



### 3.6 Effective Channel Radii

Figure 3-10 shows the frequency of effective channel radii (Eq. 7) throughout the entire simulation. The mode of radian increases when  $\tau$  decreases. With lower  $\tau$ , the conductivity of atmosphere is higher, which is advantageous for channels to spread out and connect with adjacent channels. The results suggest that the radian of 12 km for Cy method flash channels is too large in most of the cases. Most of the radian of channels is around 3 km. Only few IC and NCG channels are greater than 10km. Cy method overdamps the charge density in weak flashes and underestimates the magnitude of extreme cases. Fig. 3-11 shows that the channel of RL method is able to select an adequate region to neutralize charges. The magnitude of flashes will not saturate even in extreme cases.

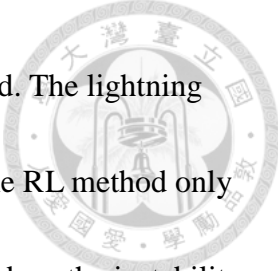


#### 4. Summary and Future Work

This study developed a cross-grid communicating discharging process. This is essential for lightning discharging process, but the numerical algorithm is incompatible to the current electricity scheme in the WRF model. It takes lots of effort to break the barrier of the grids in different parallel calculating components. With the flexibility of lightning channel geometry, both IC and CG flashes are differentiable using the proposed RL method. The RL method can also label the identical channels in different grid spacing theoretically. This is an added value of the RL discharging method.

A key contribution of this study is a clearer realization of the features of 3-dimensional charge distribution that determine the discharge of lightning. With the RL method, lightning channels adapt to an adequate geometry for involving the charged hydrometers. Instead of the thin-tube channel that branches at two ends (*MacGorman et al.* 2001), the discharging channel is more like a prolate or a dumbbell (Fig. 2-1). Like typical bulk lightning discharge, the detailed structure of lightning channel cannot be resolved within the WRF model. Charges remain in thin-tube channel is negligible in kilometer-scale grid sizes.

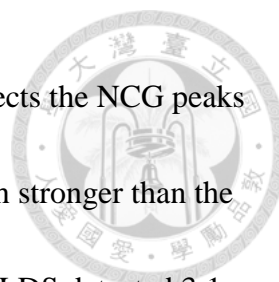
In comparison to the original WRF\_ELEC with Cy discharge, the RL method provides more realistic descriptions of the discharge processes, including polarity of CG and charge conservation of IC. The number of flashes reduced by 35% while the



neutralization is weaker in IC flashes as compared with the Cy method. The lightning flashes are charge sinks that release the instability of electric field. The RL method only neutralizes charges over unstable region, which is more efficient to reduce the instability than the Cy method. The unrealistic perturbation that would appear using the WRF\_ELEC scheme can be avoided by the channel selection strategy.

The sensitivity of  $\tau$  suggests that the prescribed radius of 12km in Cy method overestimates the size of channel and neutralizes the charges unrealistically. Unrealistic perturbation other than unstable region in Cy method can be minimized through the RL method. However, the prescribed  $\tau$  in recent model is a preliminary assumption. The real breakdown channel is determined by the conductivity of atmosphere, which is more complex than the single factor  $\tau$ .

The polarity information from the RL method reveals the relationship between lightning and microphysical features of thunderstorm. PCG flash peak indicates the initial conversion of graupel at low levels. IC flash indicates that the updraft is more than enough to produce large-size ice-phase particles at high levels. NCG flash peak occurs while the thunderstorm is decaying. Updraft in decaying thunderstorm cannot provide enough cloud drops for riming process. Then, negatively charged graupel particles fall to cloud base and induce NCG flashes. These specific events are valuable for nowcasting and are important sign for heavy precipitation. However, the polarity of



CG observed by TLDS is opposite with the RL simulated. TLDS detects the NCG peaks at initial stage and PCG at dissipating stage, and the IC peaks is much stronger than the RL method simulated. The RL simulated IC/CG ratio is 1:2.but the TLDS detected 3:1.

As it is difficult to configure the insulating factor due to the uncertainty of atmospheric conductivity, there exists inconsistency between observed and modelled IC/CG ratio.

However, the ability to differentiate between IC and CG contributes much to our understanding of the relationship between lightning and convection. By adapting IC/CG ratio as standard for regulating lightning module, discharge process can be calibrated more systematically. We look forward to simulate more weather system and perform sensitivity test on conductivity parameterization. Although the simulated sign of changes do not match with observed lightning, the experience of this study is valuable for the simulation of lightning with sophisticated geometry. By re-examine the charging mechanisms and provide more comprehensive physics description, simulations may be more comparable with observation and suitable for lightening forecast in the future.

Future work may include feedback effects on hydrometeors caused by electric fields, for example, electrophoretic force that enhances the collision efficiency of hydrometeors or changes in sedimentation speed. More case studies for other types of thunderstorm convection are also desirable for gaining a broader sense of the electrification processes. The convection current in different types of convective

systems is an important boundary condition for ideal simulation of lightning channel  
(*Pasko et al.* 1996) and thus is also worth paying attention in the future. Intensive  
observation, such as balloon-carried electric field meter, can also be arranged to provide  
more real-world verifications of model simulations.





## References



- Ballard, D. H., & Brown, C. M. (1982). *Computer vision*. Englewood Cliffs, NJ: Prentice-Hall.
- Brooks, I., Saunders, C., Mitzeva, R., & Peck, S. (1997). The effect on thunderstorm charging of the rate of rime accretion by graupel. *Atmos. Res.*,43(3), 277-295.
- Fierro, A. O., Mansell, E. R., Macgorman, D. R., & Ziegler, C. L. (2013). The Implementation of an Explicit Charging and Discharge Lightning Scheme within the WRF-ARW Model: Benchmark Simulations of a Continental Squall Line, a Tropical Cyclone, and a Winter Storm. *Mon. Wea. Rev.*,141(7), 2390-2415.
- Gardiner, B., Lamb, D., Pitter, R. L., Hallett, J., & Saunders, C. P. (1985). Measurements of initial potential gradient and particle charges in a Montana summer thunderstorm. *J. Geophys. Res.*,90(D4), 6079.
- Heiblum, R. H., Altaratz, O., Koren, I., Feingold, G., Kostinski, A. B., Khain, A. P., ... & Yaish, R. (2016). Characterization of cumulus cloud fields using trajectories in the center of gravity versus water mass phase space: 2. Aerosol effects on warm convective clouds. *Journal of Geophysical Research: Atmospheres*, 121(11), 6356-6373.
- Helsdon, J. H., Wu, G., & Farley, R. D. (1992). An intracloud lightning parameterization scheme for a storm electrification model. *J. Geophys. Res. Atmos.*, 97(D5),



5865-5884.

Jayarathne, E., Saunders, C., & Hallett, J. (1983). Laboratory studies of the charging of soft-hail during ice crystal interactions. *Q. J. Roy. Meteor. Soc.*,109(461), 609-630.

Krehbiel, P. R. (1986). The electrical structure of thunderstorms. *The Earth's electrical environment*, 90-113.

Macgorman, D. R., Straka, J. M., & Ziegler, C. L. (2001). A Lightning Parameterization for Numerical Cloud Models. *J. Appl. Meteorol.*,40(3), 459-478.

Mansell, E. R., Macgorman, D. R., Ziegler, C. L., & Straka, J. M. (2002). Simulated three-dimensional branched lightning in a numerical thunderstorm model. *J. Geophys. Res. Atmos.*,107(D9).

Mansell, E. R., MacGorman, D. R., Ziegler, C. L., & Straka, J. M. (2005). Charge structure and lightning sensitivity in a simulated multicell thunderstorm. *J. Geophys. Res. Atmos.*, 110(D12).

Niemeyer, L., Pietronero, L., & Wiesmann, H. J. (1984). Fractal dimension of dielectric breakdown. *Phys. Rev. Lett.*, 52(12), 1033.

Pasko, V. P., Inan, U. S., & Bell, T. F. (1996). Sprites as luminous columns of ionization produced by quasi-electrostatic thundercloud fields. *Geophys. Res. Lett.*, 23(6), 649-652.

Ritenour, A. E., Morton, M. J., McManus, J. G., Barillo, D. J., & Cancio, L. C. (2008).



- Lightning injury: a review. *Burns*, 34(5), 585-594.
- Saunders, C. P., & Peck, S. L. (1998). Laboratory studies of the influence of the rime accretion rate on charge transfer during crystal/graupel collisions. *J. Geophys. Res. Atmos.*, 103(D12), 13949-13956.
- Saunders, C. P. (2008). Charge separation mechanisms in clouds. In *Planetary Atmospheric Electricity* (pp. 335-353). Springer, New York, NY.
- Skamarock, W. C., Klemp, J. B., Dudhia, J., Gill, D. O., Barker, D. M., Duda, M. G., ... & Powers, J. G. (2008). A Description of the Advanced Research WRF Version 3.
- Stolzenburg, M., W. D. Rust, and T. C. Marshall (1998), Electrical structure in thunderstorm convective regions: 3. Synthesis, *J. Geophys. Res.*, 103(D12), 14097–14108.
- Tai, J. H., Wang, Y. M., Yang, M. J. & Lin, P. H. (2017) The preliminary study of applying intra-cloud lightning data to convective rain fall nowcasting. *大氣科學*, 45(1), 43-56。
- Takahashi, T. (1978). Riming electrification as a charge generation mechanism in thunderstorms. *J. Atmos. Sci.*, 35(8), 1536-1548.
- Tsai, W., & Wu, C. (2017). The environment of aggregated deep convection. *J. Adv. Model. Earth Sy.*, 9(5), 2061-2078.
- Wiesmann, H. J., & Zeller, H. R. (1986). A fractal model of dielectric breakdown and

prebreakdown in solid dielectrics. *J. Appl. Phys.*, 60(5), 1770-1773.

Zhang, R., Tie, X., & Bond, D. W. (2003). Impacts of anthropogenic and natural NO<sub>x</sub> sources over the U.S. on tropospheric chemistry. *P. Natl. Acad. Sci. U.S.A.*, 100(4), 1505-1509

Ziegler, C. L., Macgorman, D. R., Dye, J. E., & Ray, P. S. (1991). A model evaluation of noninductive graupel-ice charging in the early electrification of a mountain thunderstorm. *J. Geophys. Res.*, 96(D7), 12833.



## Figures

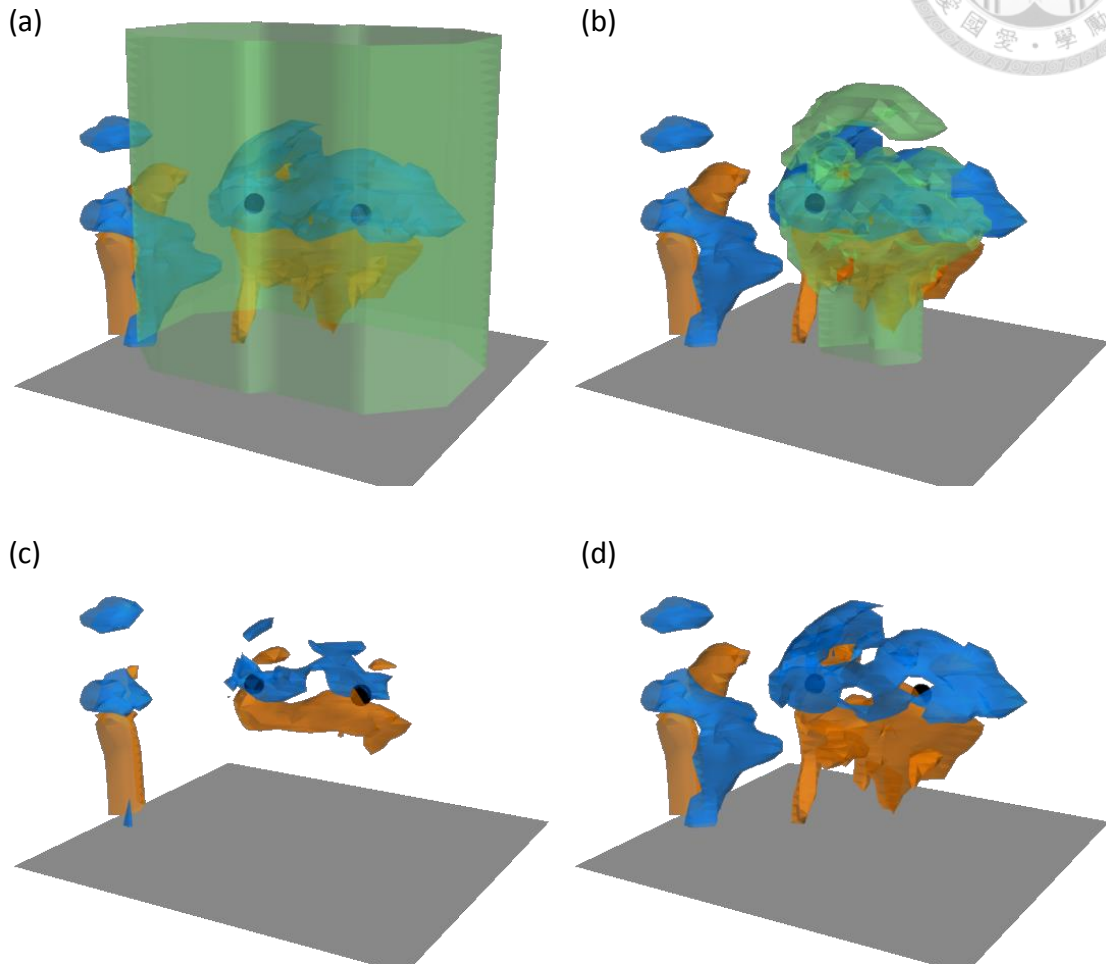


Figure 2-1: A three-dimensional view of the discharge using the Cy method (a, c) and the RL method (b, d). Upper panels show the region with significant positive charges (orange) and negative charges (blue); the discharge regions are indicated with green-shading areas. Lower panels are charge distribution after flash.

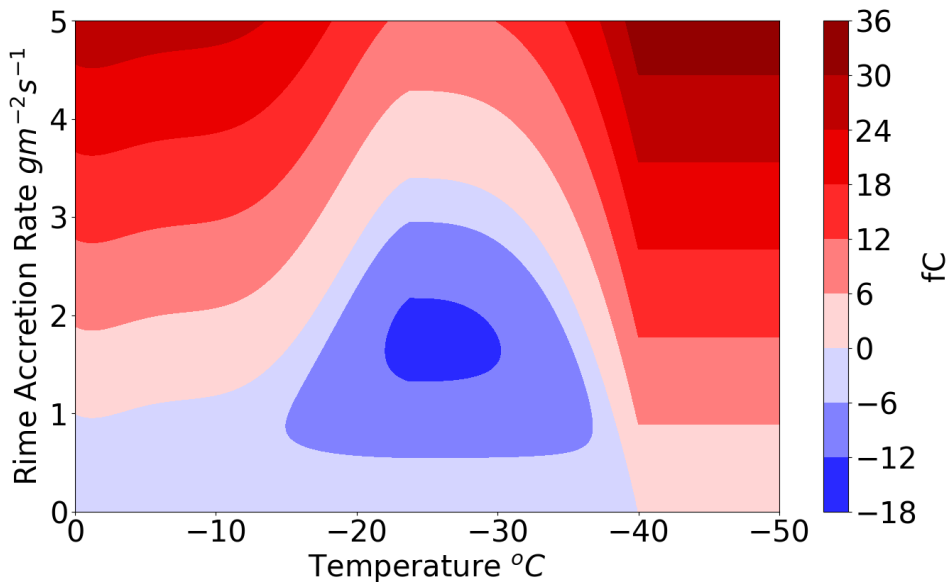


Figure 2-2: The charge attached on graupel per-collision with ice/snow particle. The values below  $-40^{\circ}\text{C}$  are invalid and are filtered out during model iteration. *Mansell et al. (2005)*

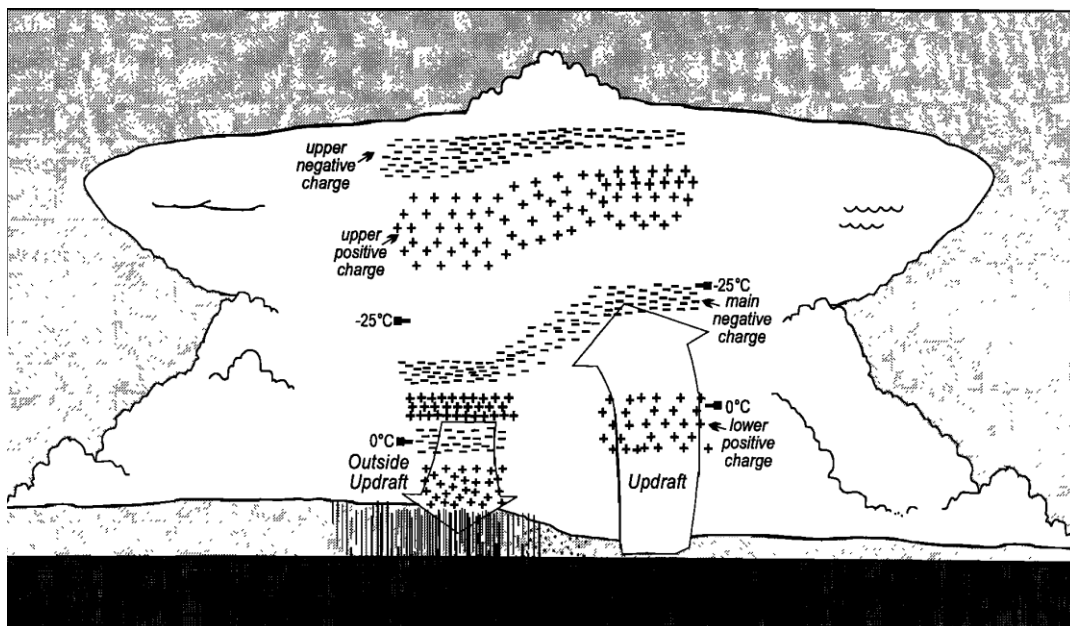


Figure 2-3: Schematic of the basic charge distribution in the convective region of thunderstorm. *(Stolzenburg et al. 1998)*

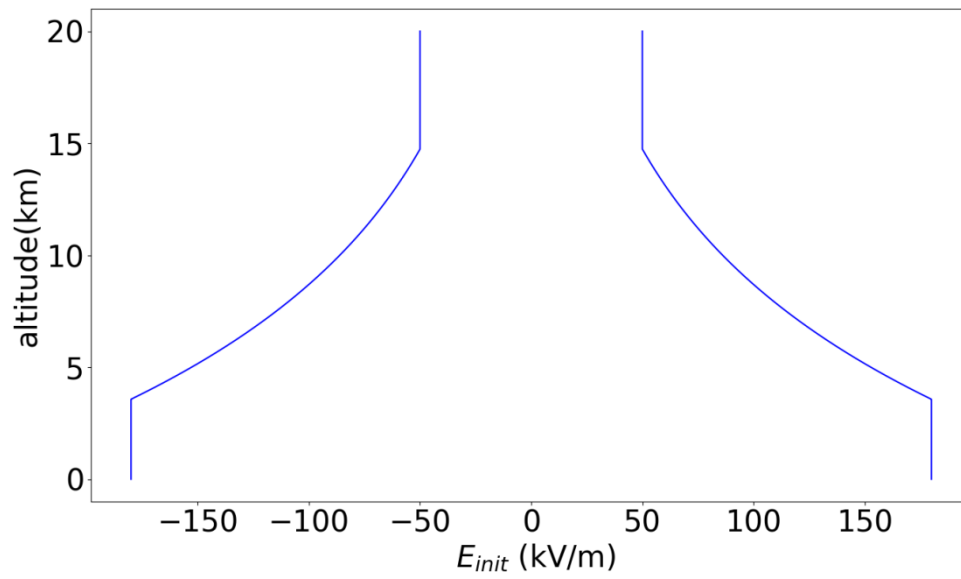


Figure 2-4: The critical electric field for diagnosis of initial points of lightning. This is a demonstration of isothermal atmosphere with 293K.

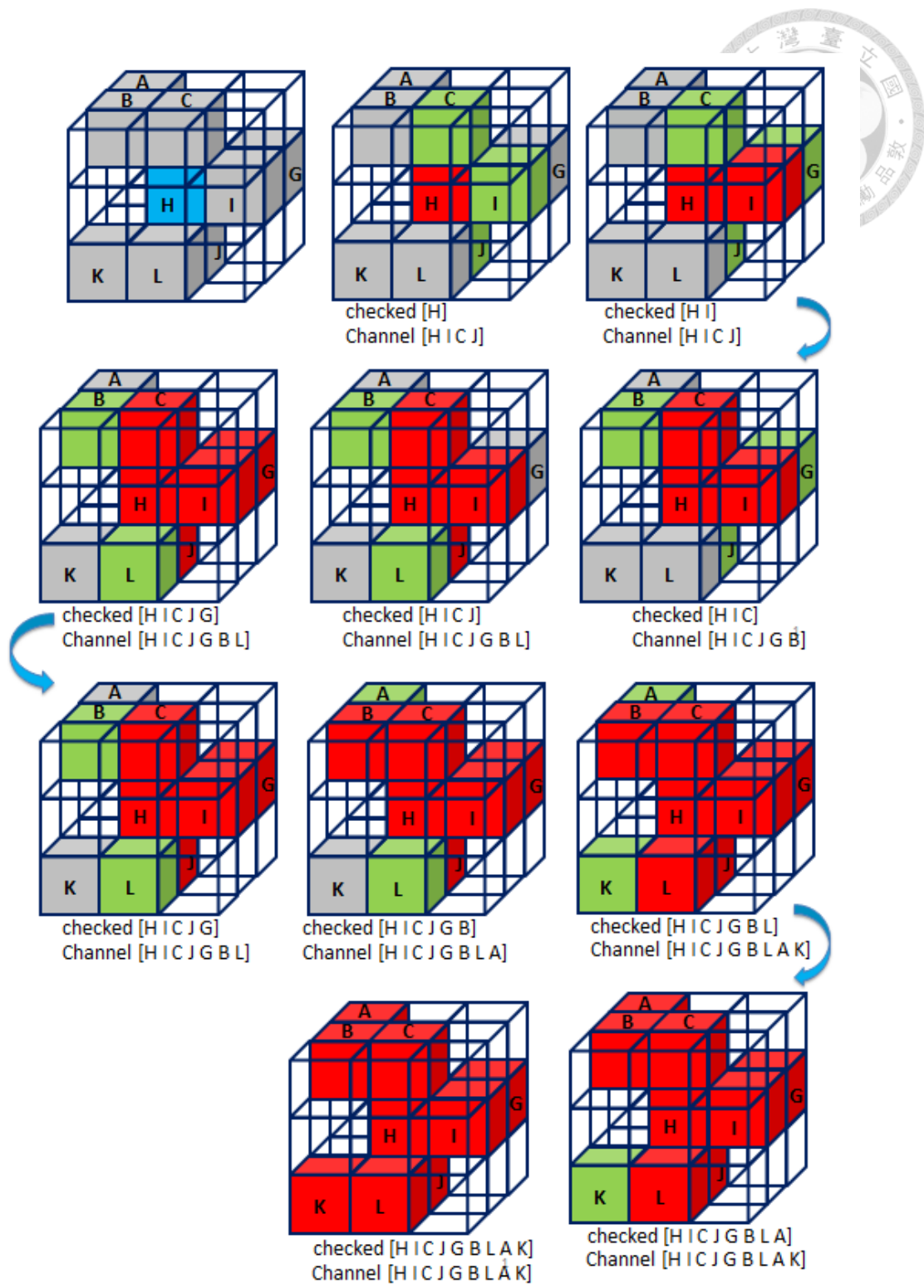


Figure 2-5: A demonstration of RL method labels an individual channel. Blue grid is the initial grid with electric field magnitude greater than  $E_{init}$ . Gray grids are the grids with electric field greater than  $\tau E_{init}$ , which is the potential to join the channel. Red grids are grids which have been checked by RL method. Green grids are contiguous grids that join the channel. The algorithm terminates while all of the grids in the channel have been checked by RL method.



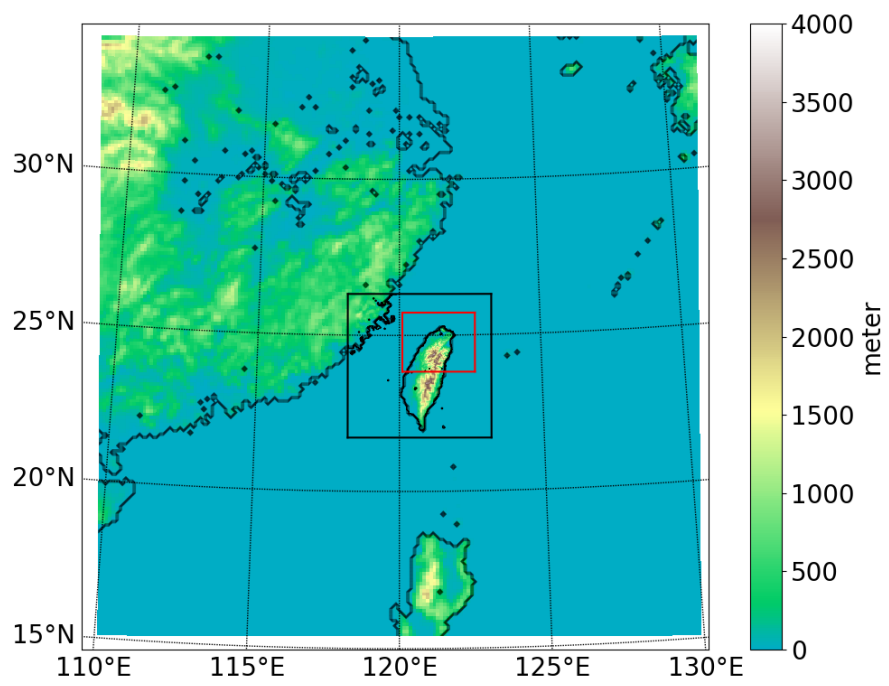


Figure 2-6: Domain configuration of the WRF model. Black block region is the nested second domain with 4 km grid spacing. Red block is the nested third domain with 4/3 km grid spacing.

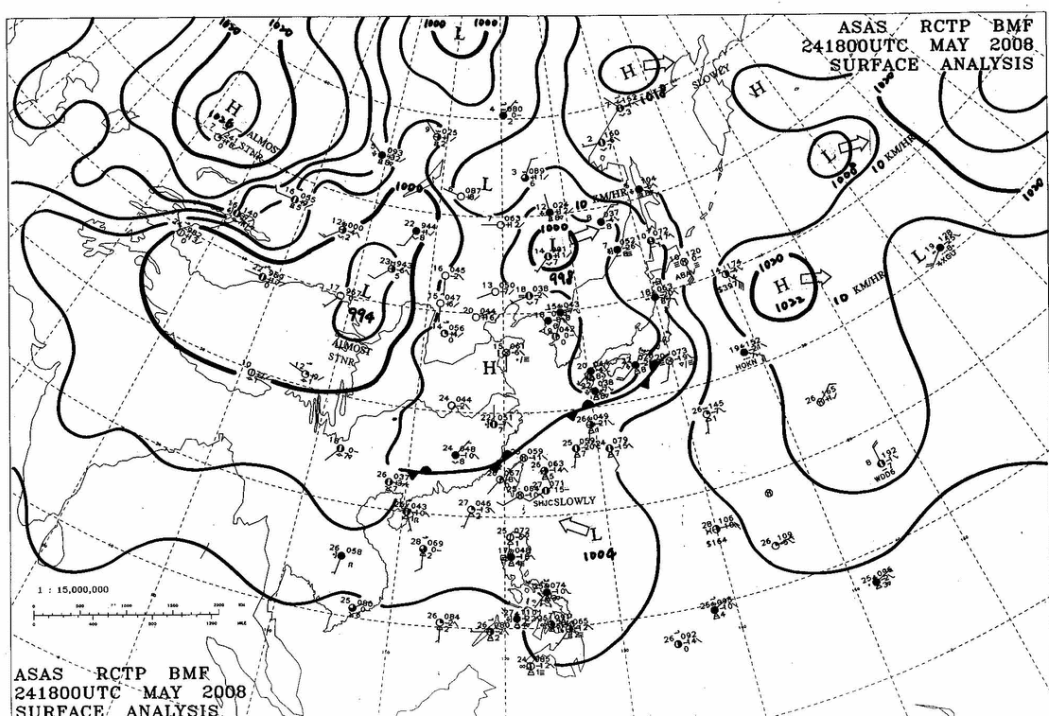


Figure 2-7: Synoptic weather chart at initial time of simulation, 1800 UTC, May 24<sup>th</sup>, 2008

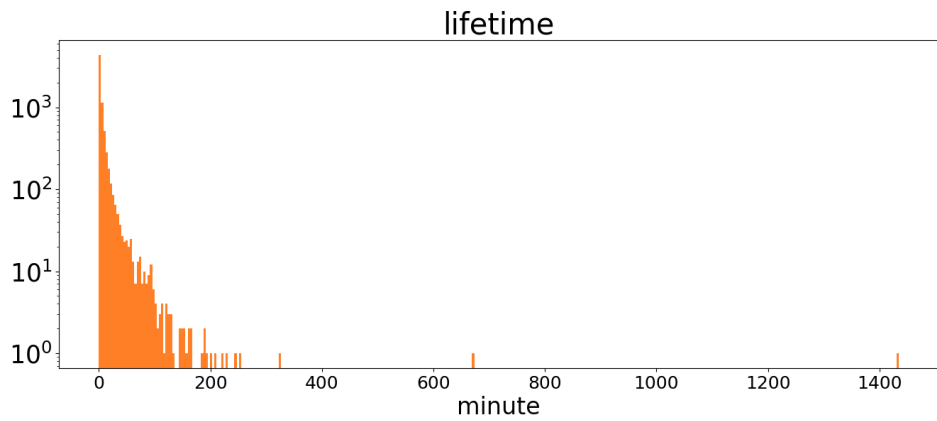
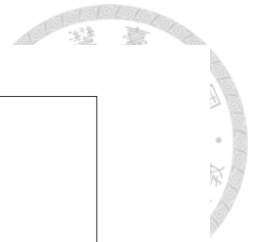


Figure 3-1: Frequency of independent cloud series lifetime.

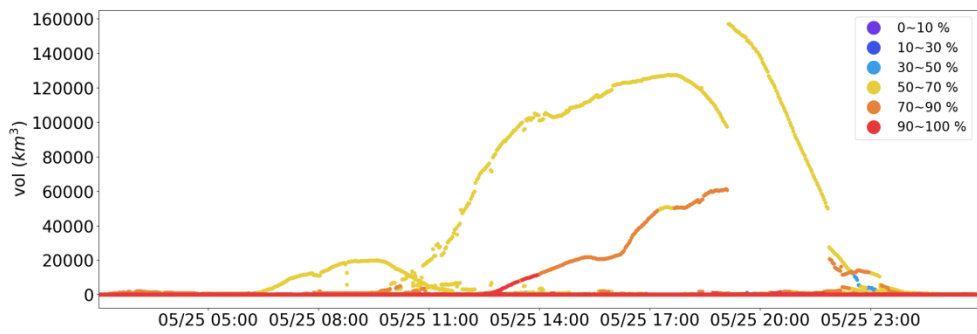
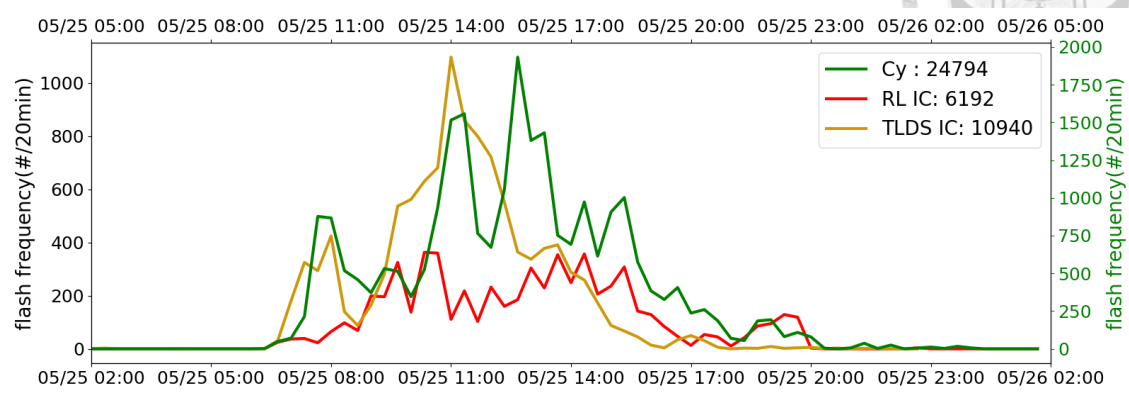


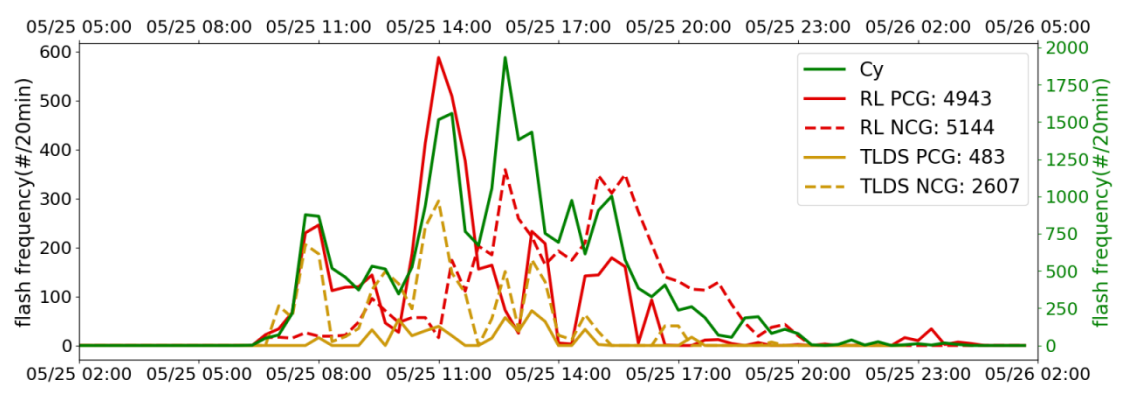
Figure 3-2: Evolution of the main cloud series. Each dot is a contiguous cloud segment. Colors denote the volume ratio of upward motion of each cloud segment.



(a)



(b)



(c)

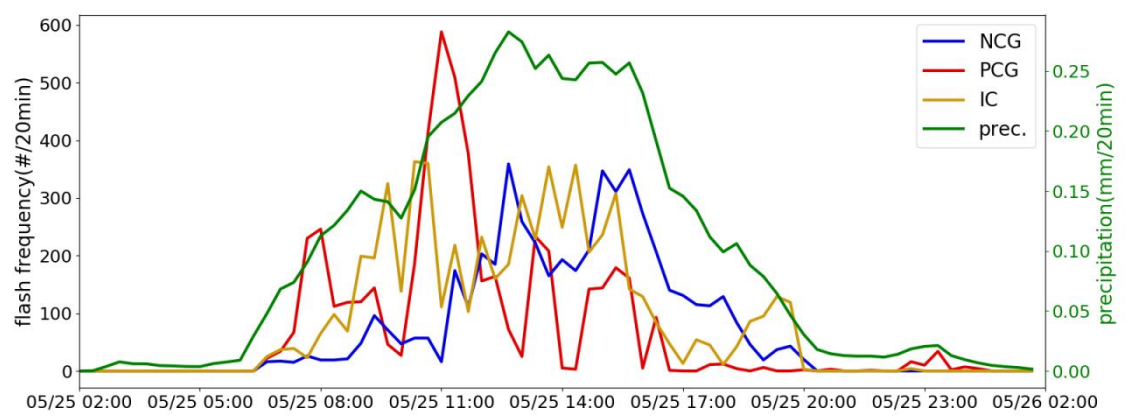


Figure 3-3: Time series of IC (a) and CG (b) frequency, and flashes overlapped with domain-averaged precipitation (c). The total number of flashes through the entire simulation is noted at legend. Note that Cy only simulate total flashes which makes no difference between IC and CG. The scales of RL and observed flashes are shown on the left axis, whereas that of Cy is shown on the right axis. The time axis of observation is shifted and labeled at the upper axis.

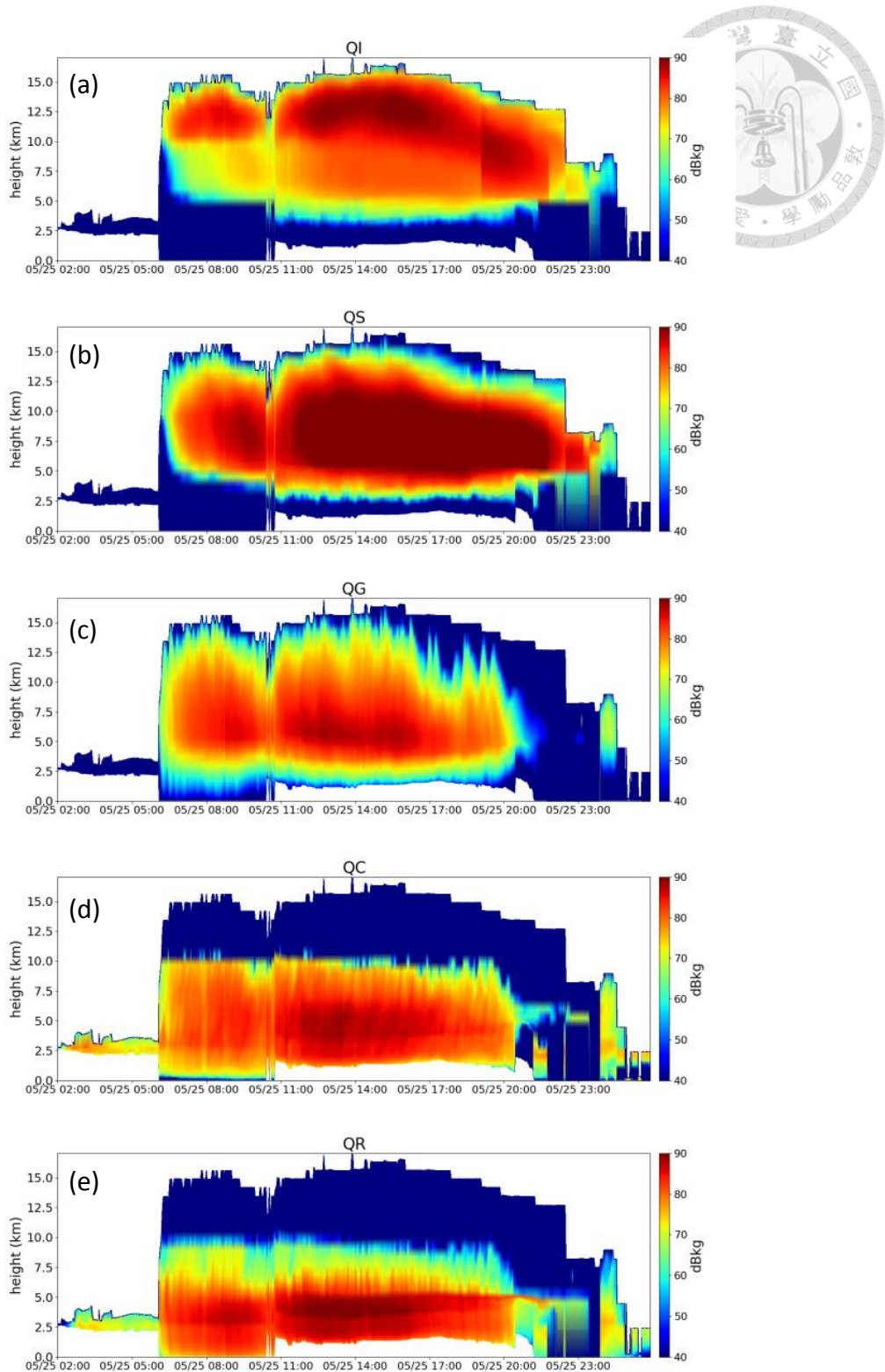


Figure 3-4: Evolution of the vertical profile of hydrometeor contents in one of the largest thunderstorm cell. The cell is determined by 0.1 g/kg condensed phase water contiguous region with similar RL approach. QI: cloud ice; QS: snow; QG: graupel; QC: cloud drop; QR: rain drop

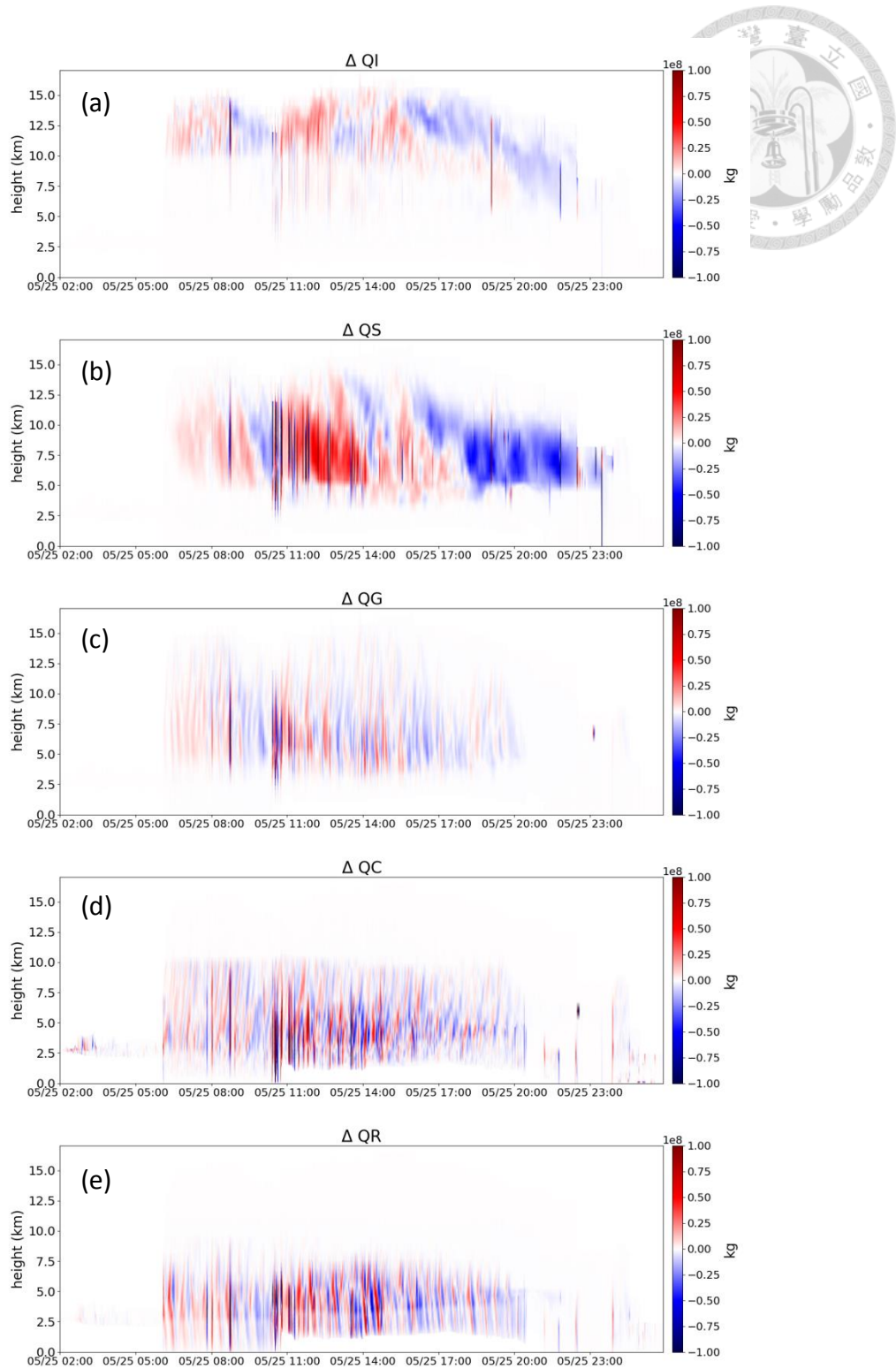


Figure 3-5: Similar to Figure 3-4, excepts it shows the tendency of hydrometeor contents.

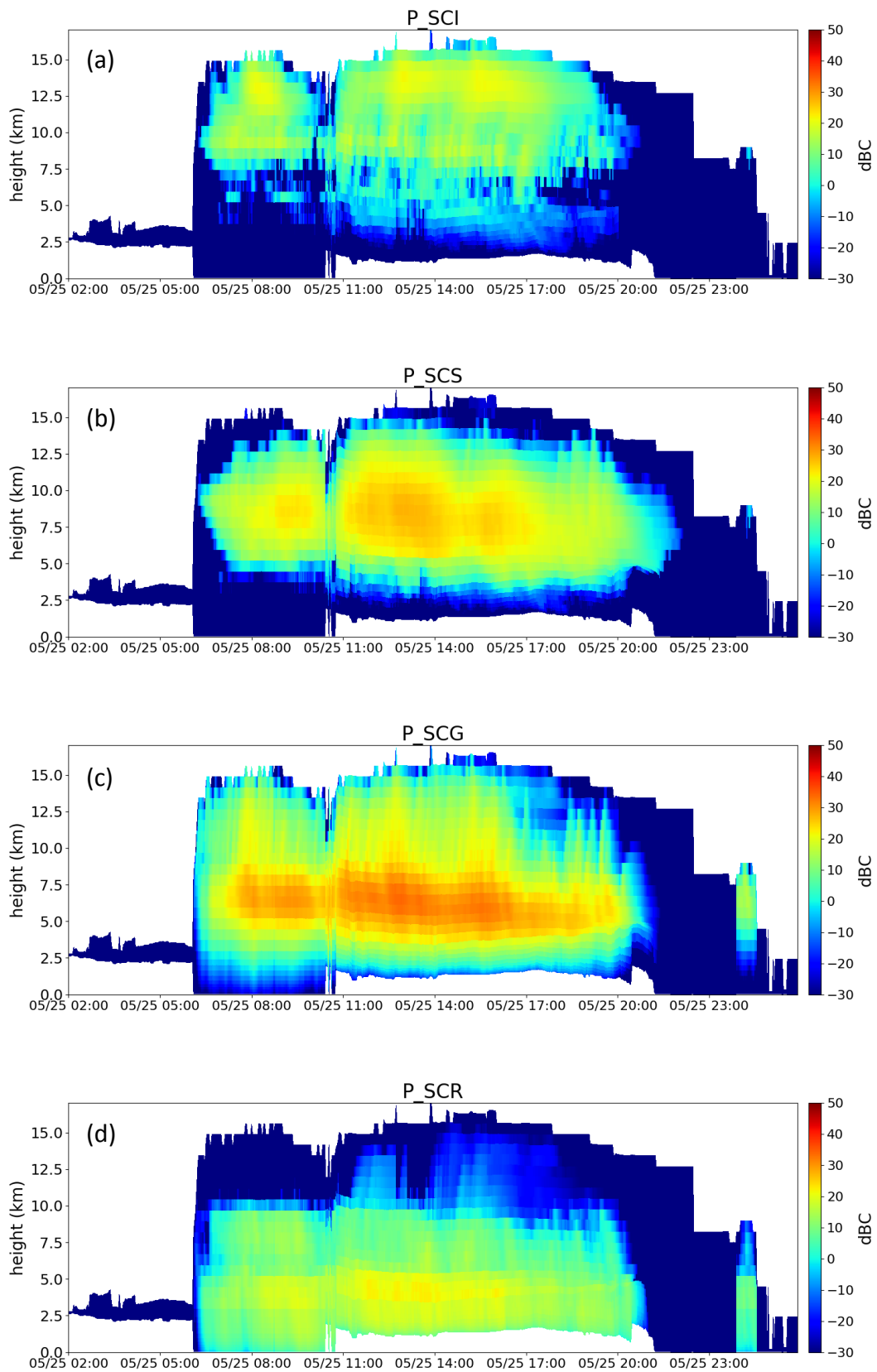
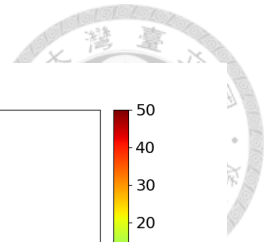


Figure 3-6: Similar to Figure 3-4, excepts it shows the cumulative positive charge attached on hydrometeors.

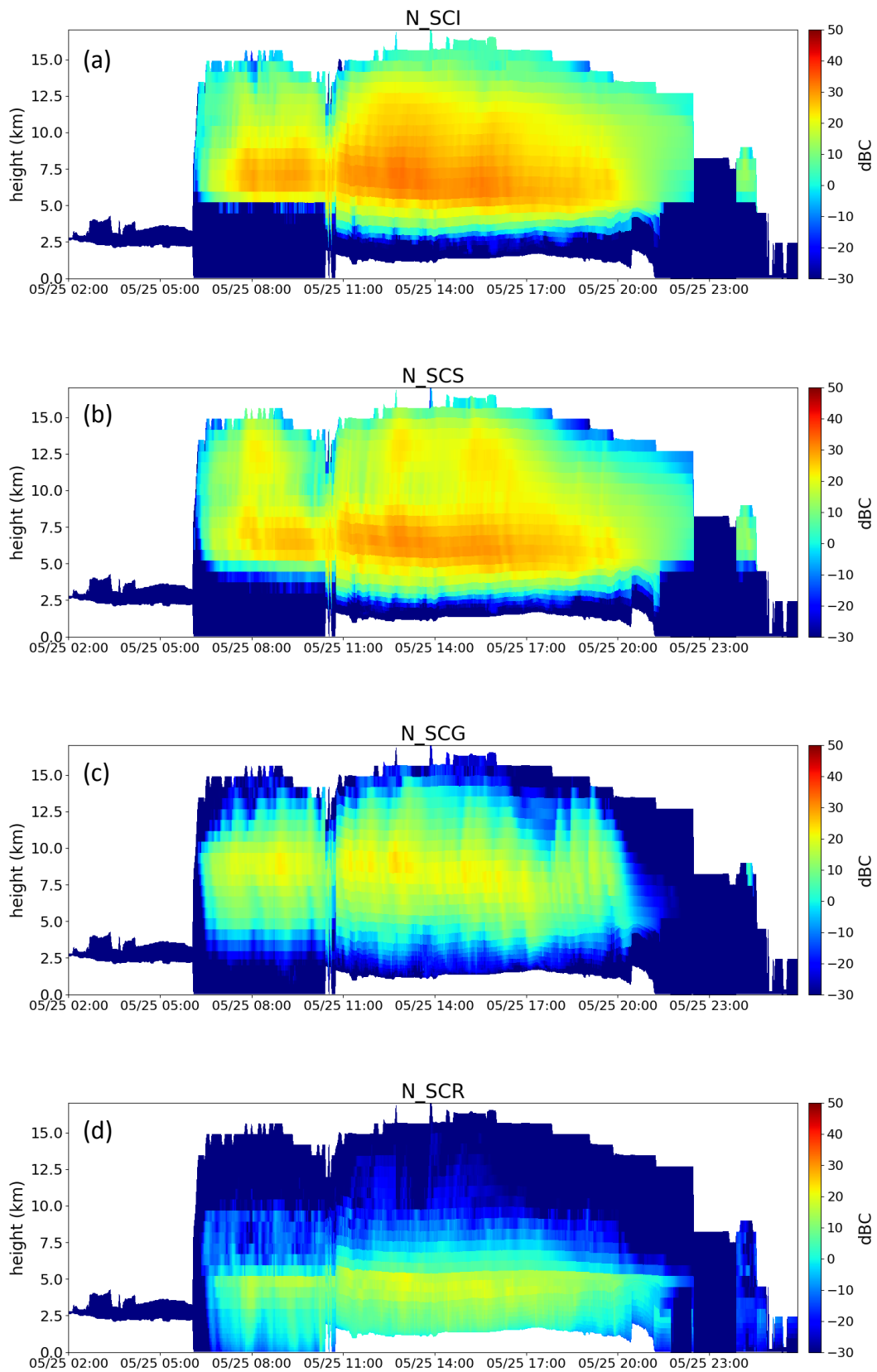
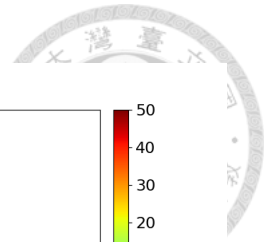


Figure 3-7: Similar to Figure 3-4, excepts it shows the cumulative negative charge attached on hydrometeors.

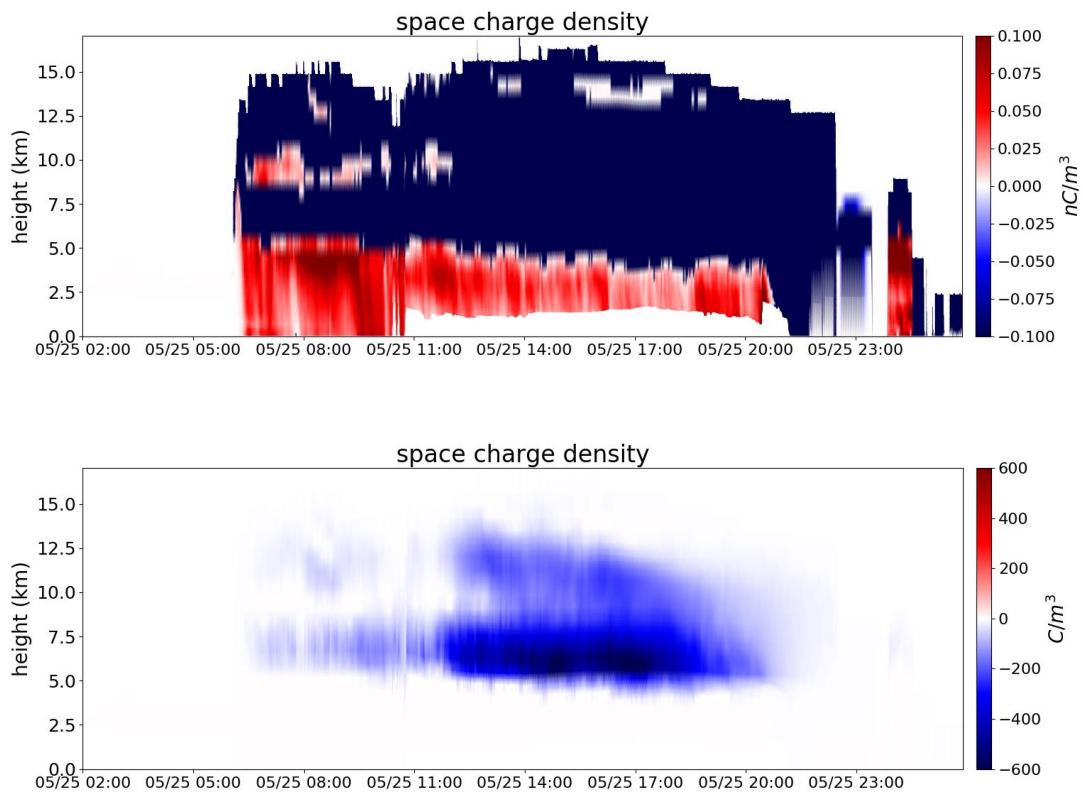
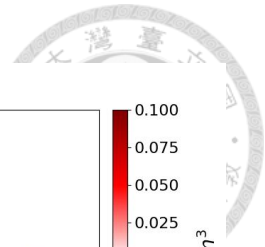


Figure 3-8: Similar to Figure 3-4, excepts it shows the average space charge density. Top: customized colorbar for positive charges; bottom: customized colorbar for negative charges.



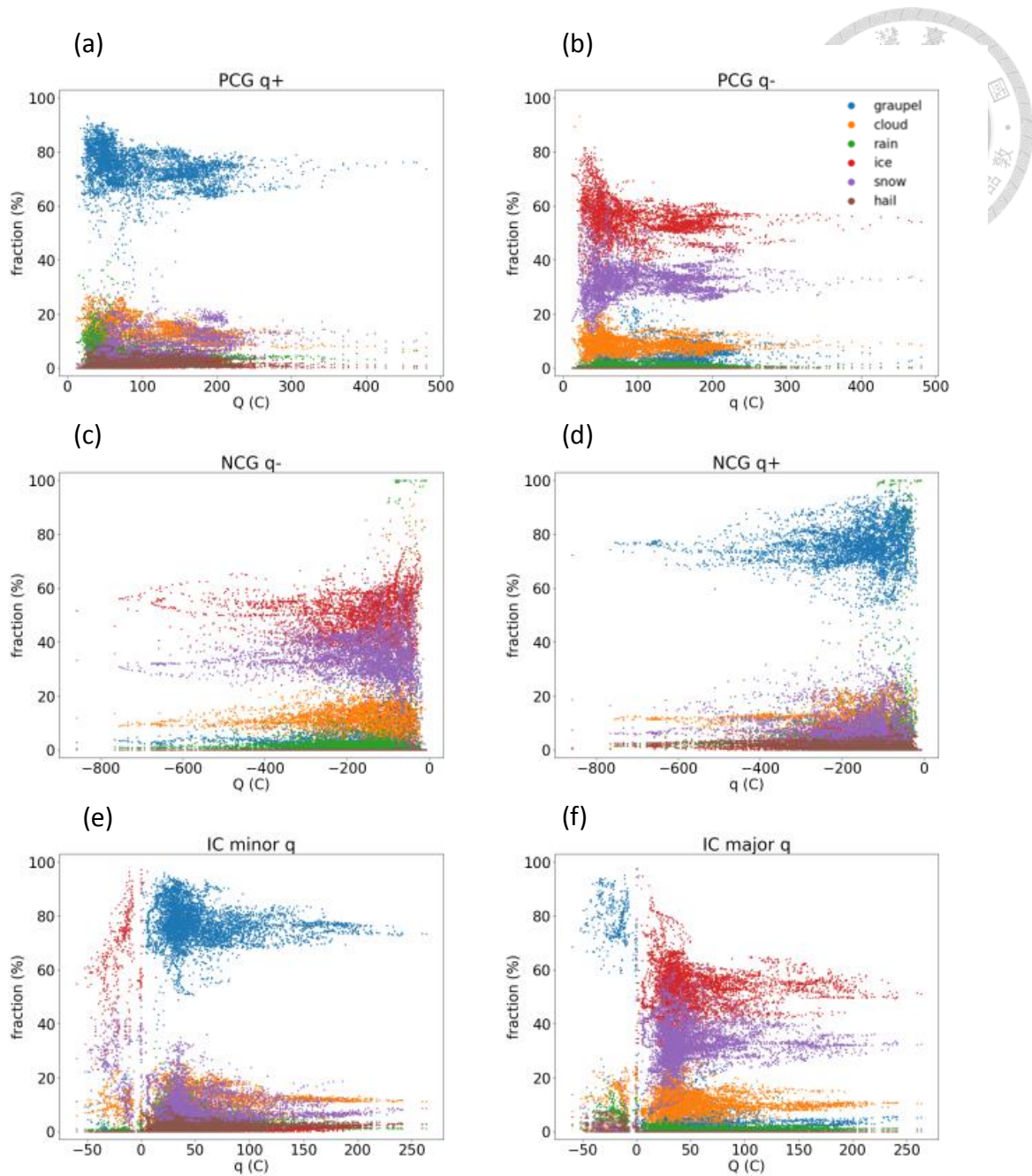


Figure 3-9: Proportion of charges carried by hydrometeors in three types of flashes. Left panels (a, c, e) are the limiting reagent of lighting: positive charges for PCG (a), negative charges for NCG (c) and minor charges for IC (e). Right panels (b, d, f) are opposite-sign charges. Horizontal axis is the electric quantity of the limiting reagent which determines the magnitude of neutralization.

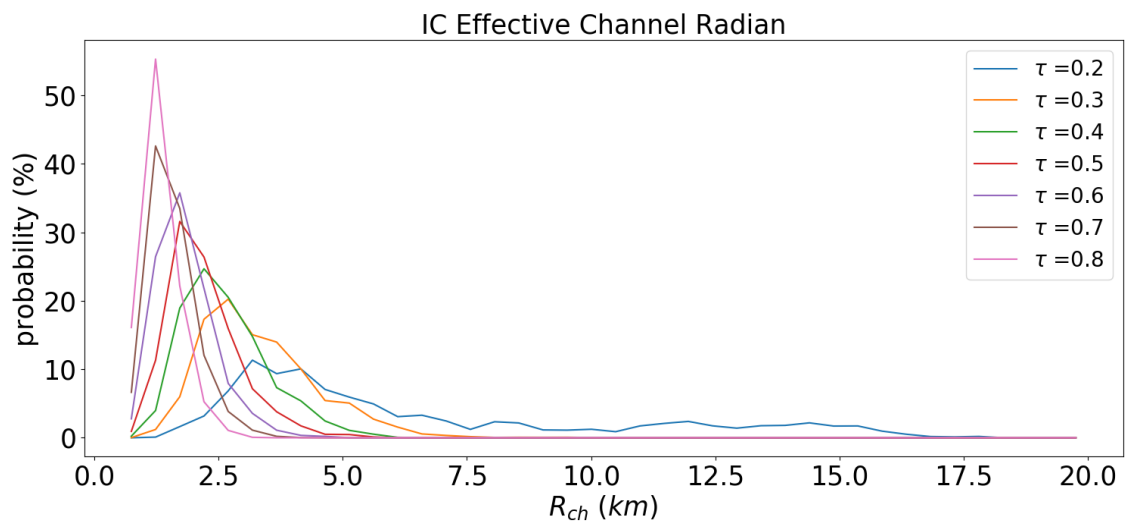
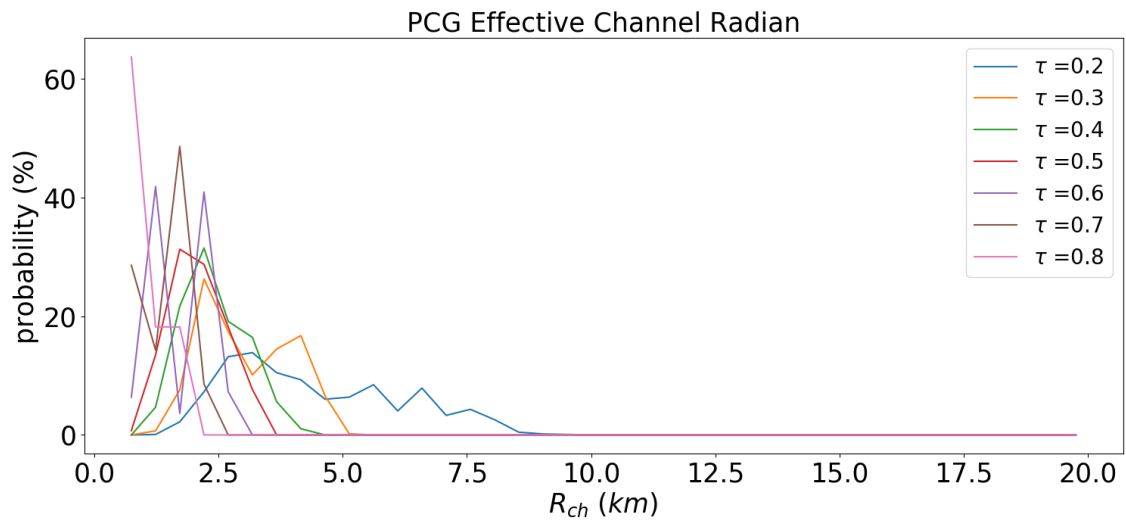
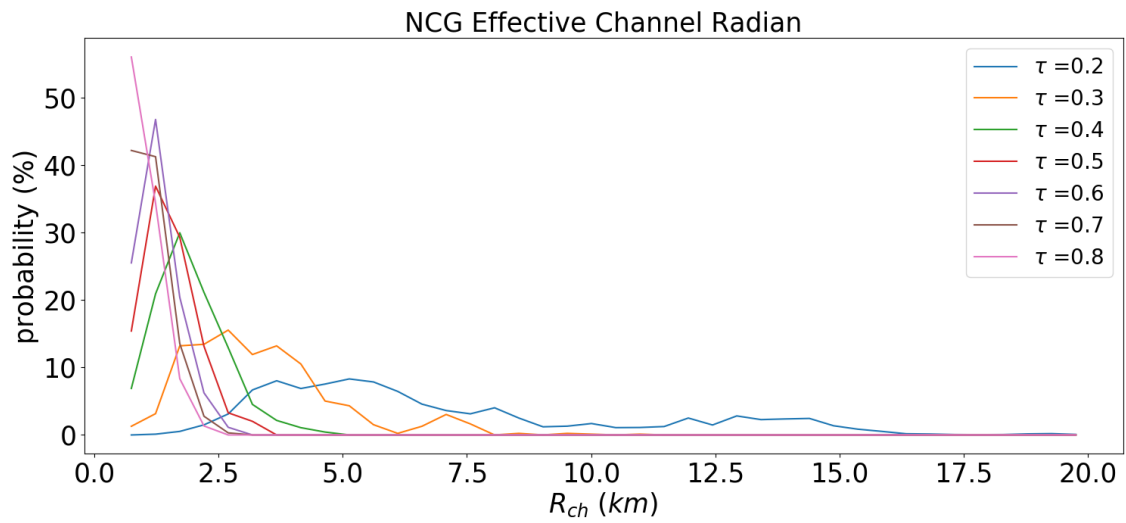
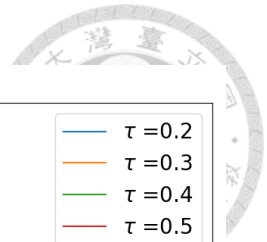


Figure 3-10: Frequency of effective channel radii under different insulating factor scenario.

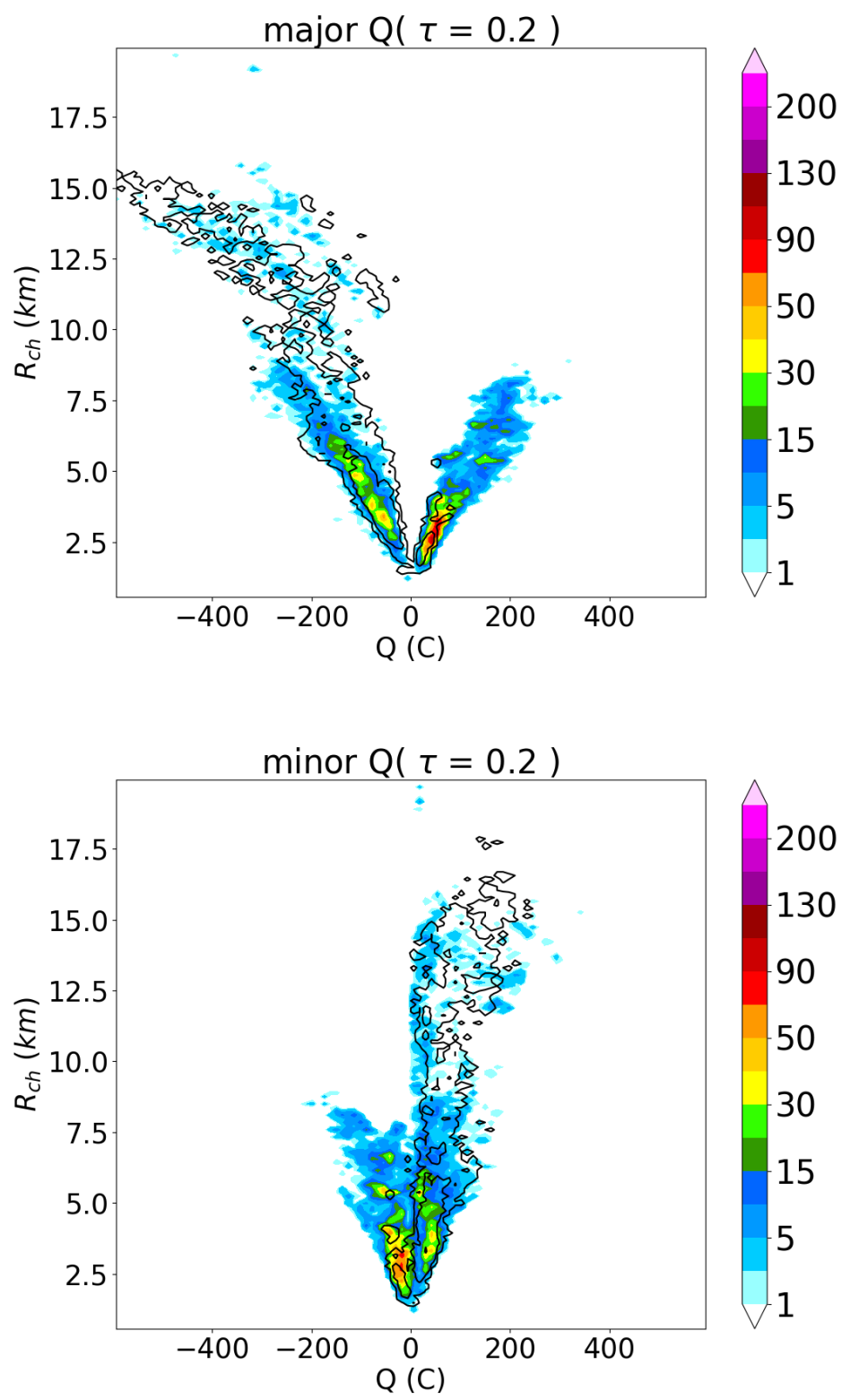


Figure 3-11: Relation between effective channel radii and quantity of electric charge inside channel. Shading denotes the CG counts. Contour denotes the IC counts with values of 1, 10, 100, 1000.



## Table

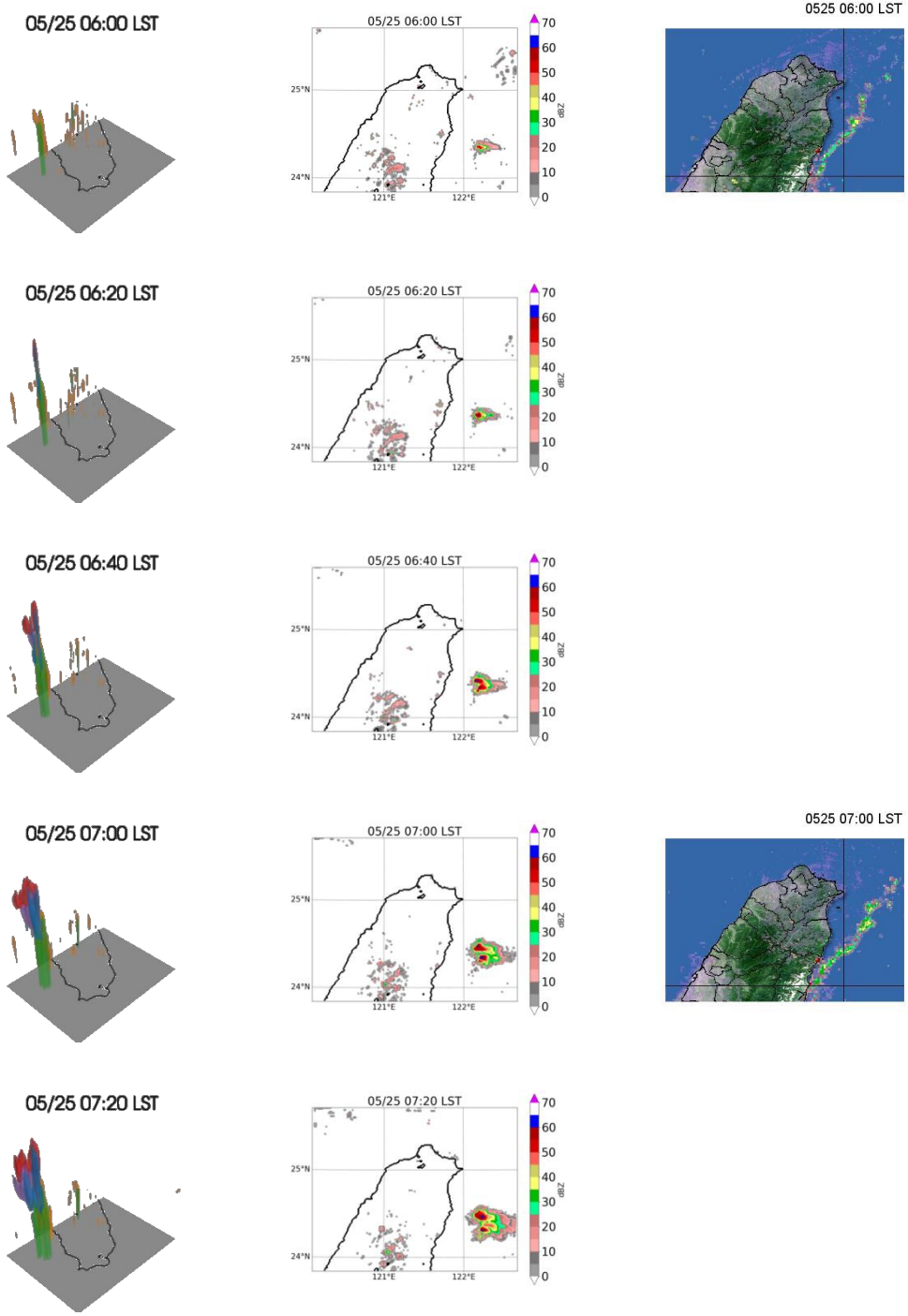
Table 1: Notable option of the WRF model as used this study.

<b>Simulation Period</b>	
20080524 18Z ~ 20080525 18Z (24 hrs)	
<b>Domains setting</b>	
Domain 1	180 × 180 (12 km) 30s
Domain 2	130 × 130 (4 km) 10s
Domain 3	196 × 160 (1.33 km) 3.33s
Vertical	50 layers; $P_{top} = 10$ hPa
<b>Physics Options</b>	
Cumulus	Kain-Fritsch (D1 only)
PBL	YSU
SW radiation	New Goddard
LW radiation	New Goddard
Surface layer	MM5 similarity
Land surface	5-layer thermal diffusion
Microphysics	NSSL 2-moment 4-ice scheme (steady background CCN)

# Appendix

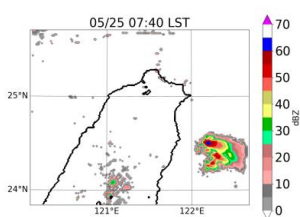
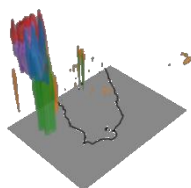


## Appendix A1: Composite reflectivity and three-dimensional view of the convective cells.

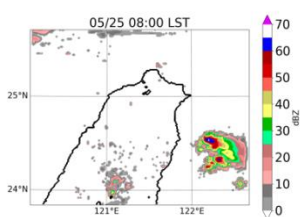
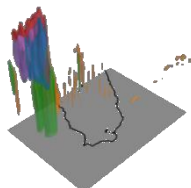




05/25 07:40 LST



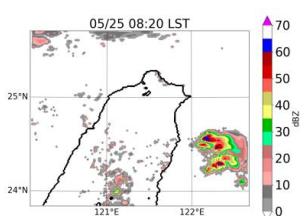
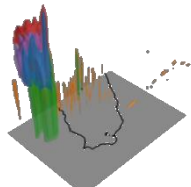
05/25 08:00 LST



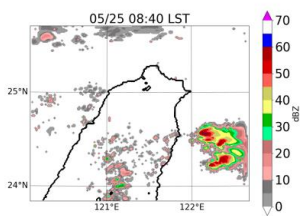
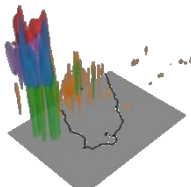
0525 08:00 LST



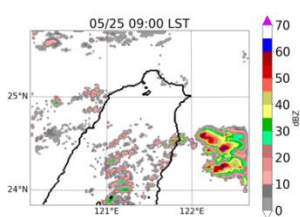
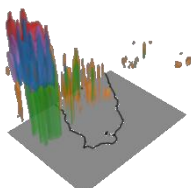
05/25 08:20 LST



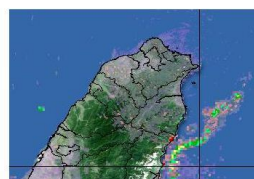
05/25 08:40 LST



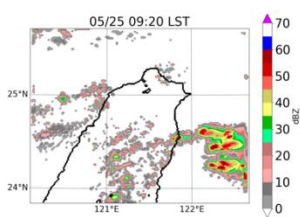
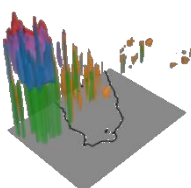
05/25 09:00 LST



0525 09:00 LST

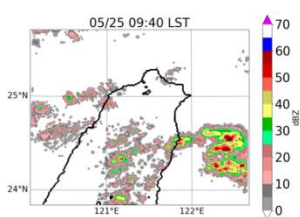
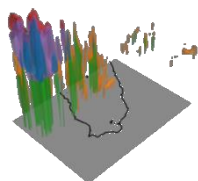


05/25 09:20 LST

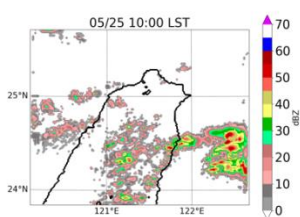
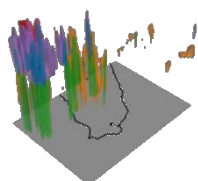




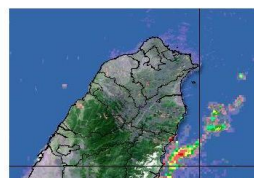
05/25 09:40 LST



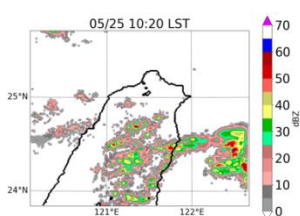
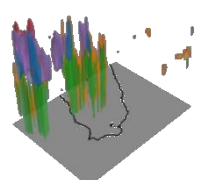
05/25 10:00 LST



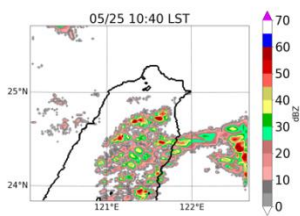
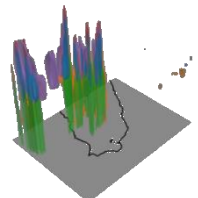
0525 10:00 LST



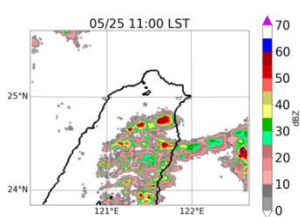
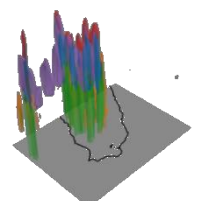
05/25 10:20 LST



05/25 10:40 LST



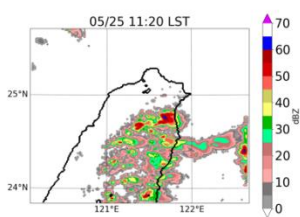
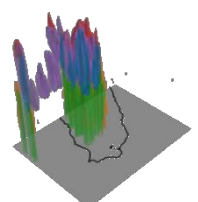
05/25 11:00 LST



0525 11:00 LST

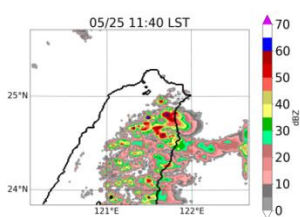
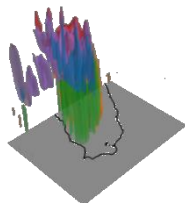


05/25 11:20 LST

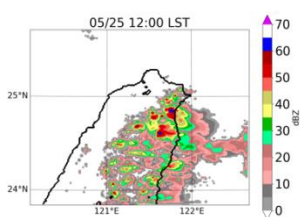
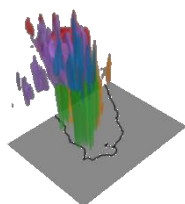




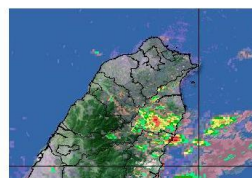
05/25 11:40 LST



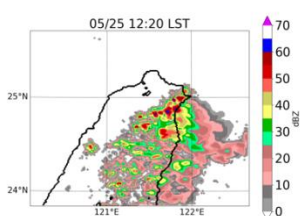
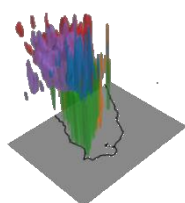
05/25 12:00 LST



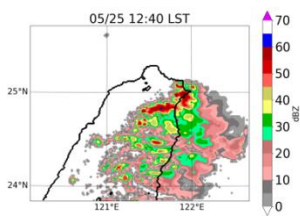
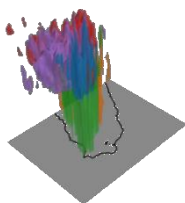
0525 12:00 LST



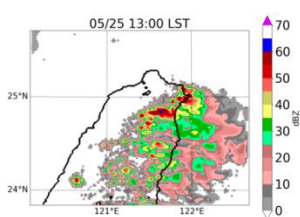
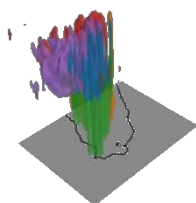
05/25 12:20 LST



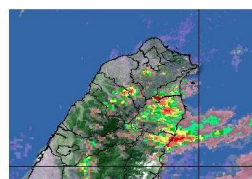
05/25 12:40 LST



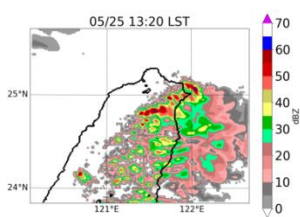
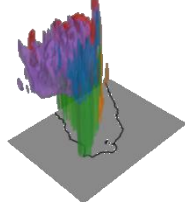
05/25 13:00 LST



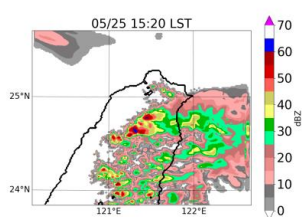
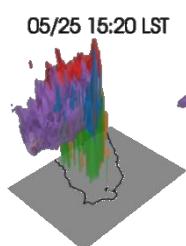
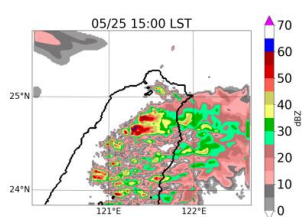
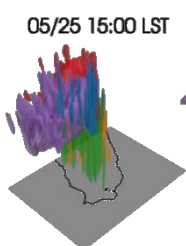
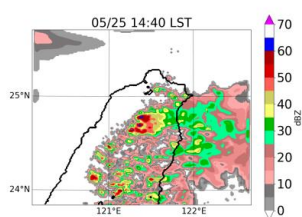
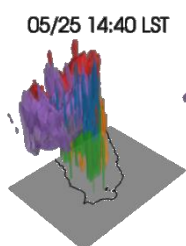
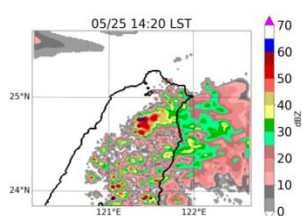
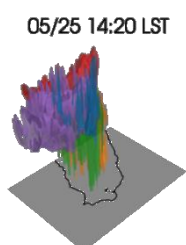
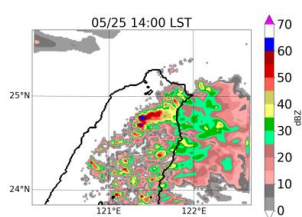
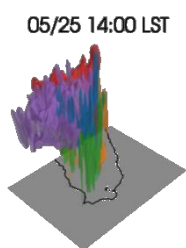
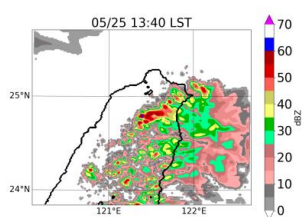
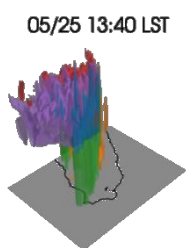
0525 13:00 LST

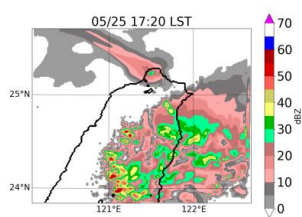
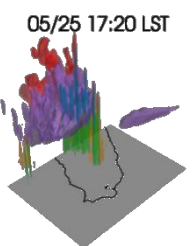
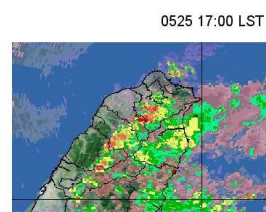
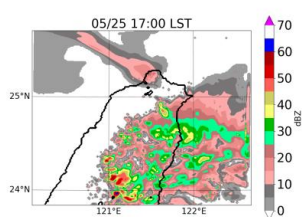
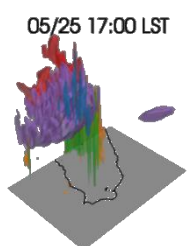
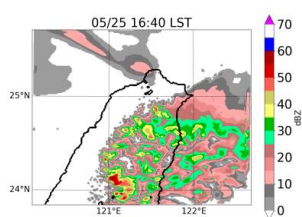
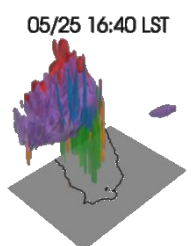
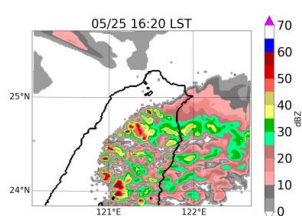
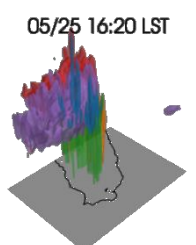
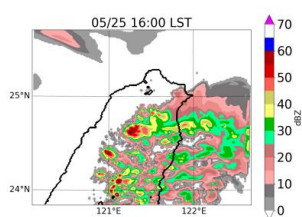
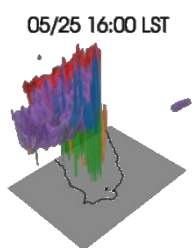
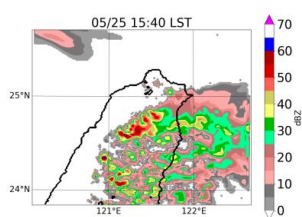
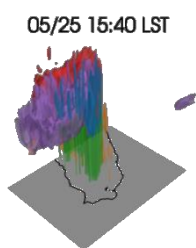


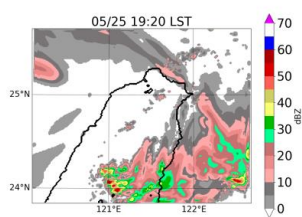
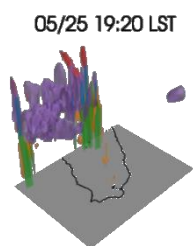
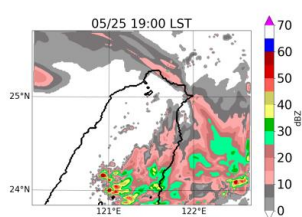
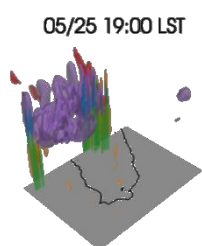
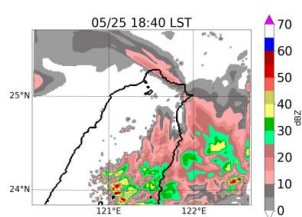
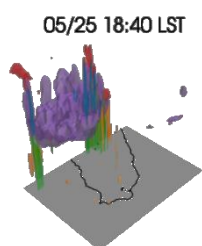
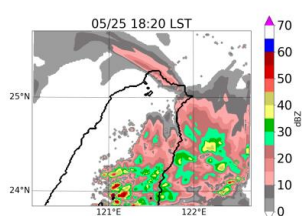
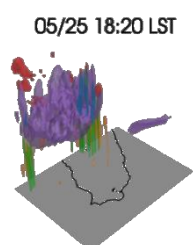
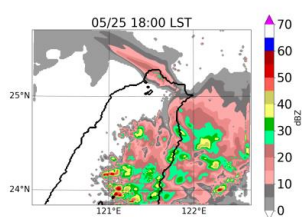
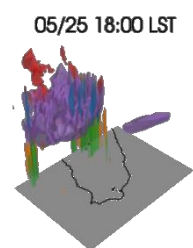
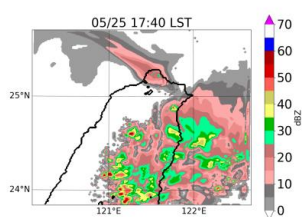
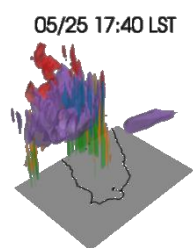
05/25 13:20 LST











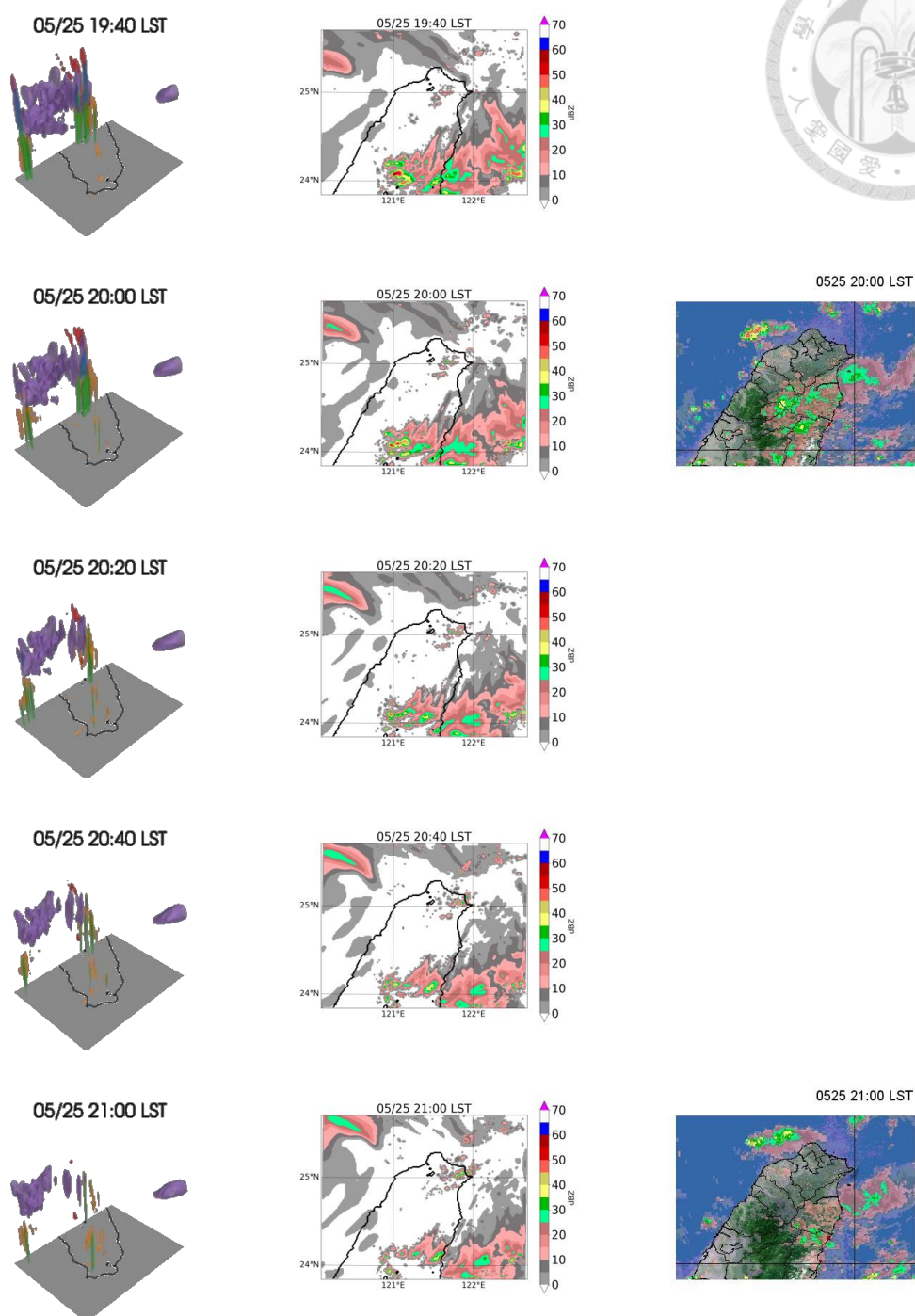
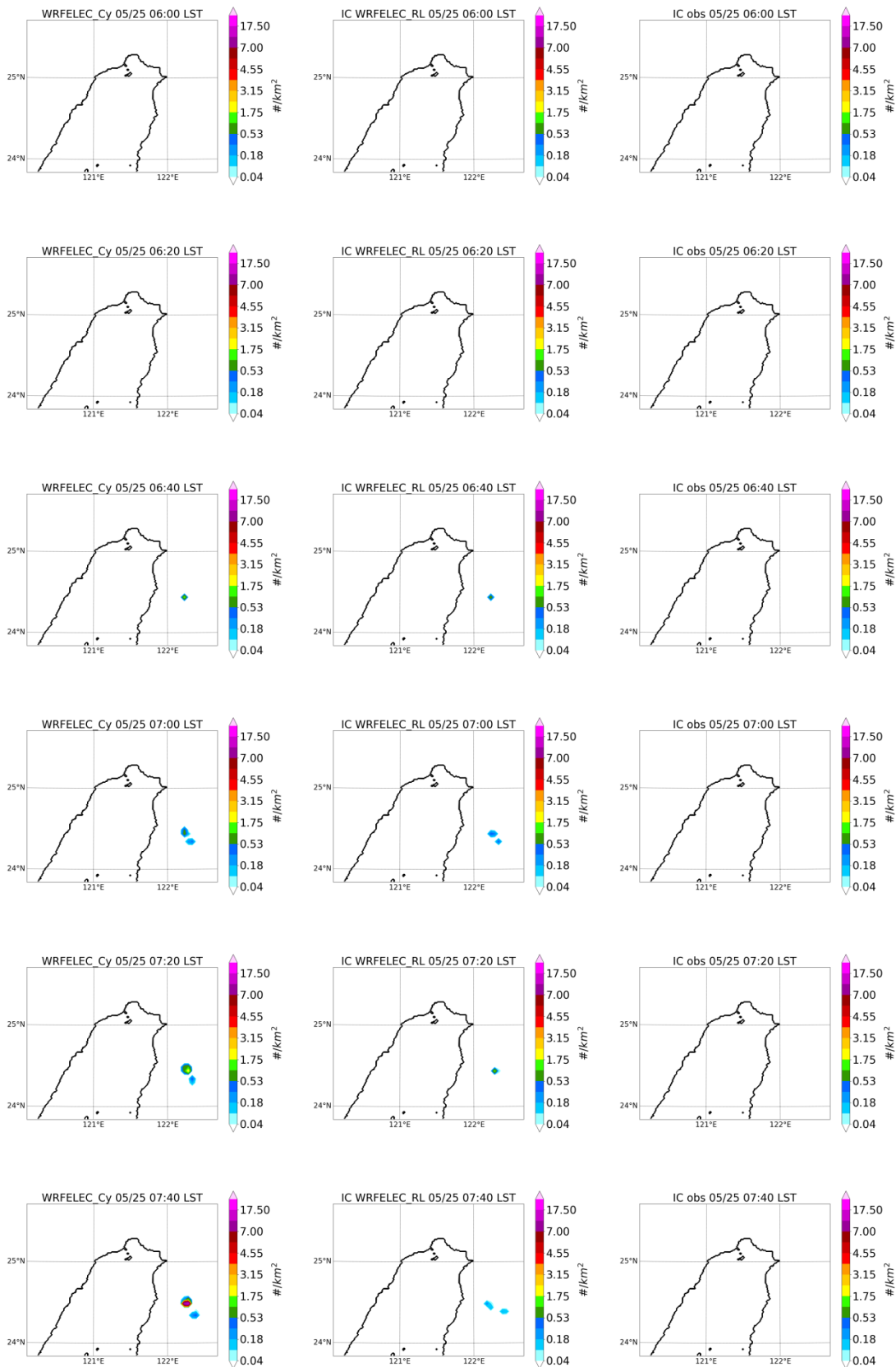
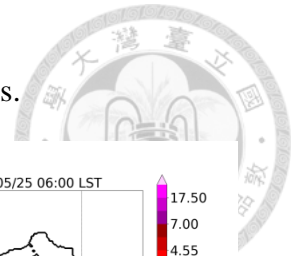
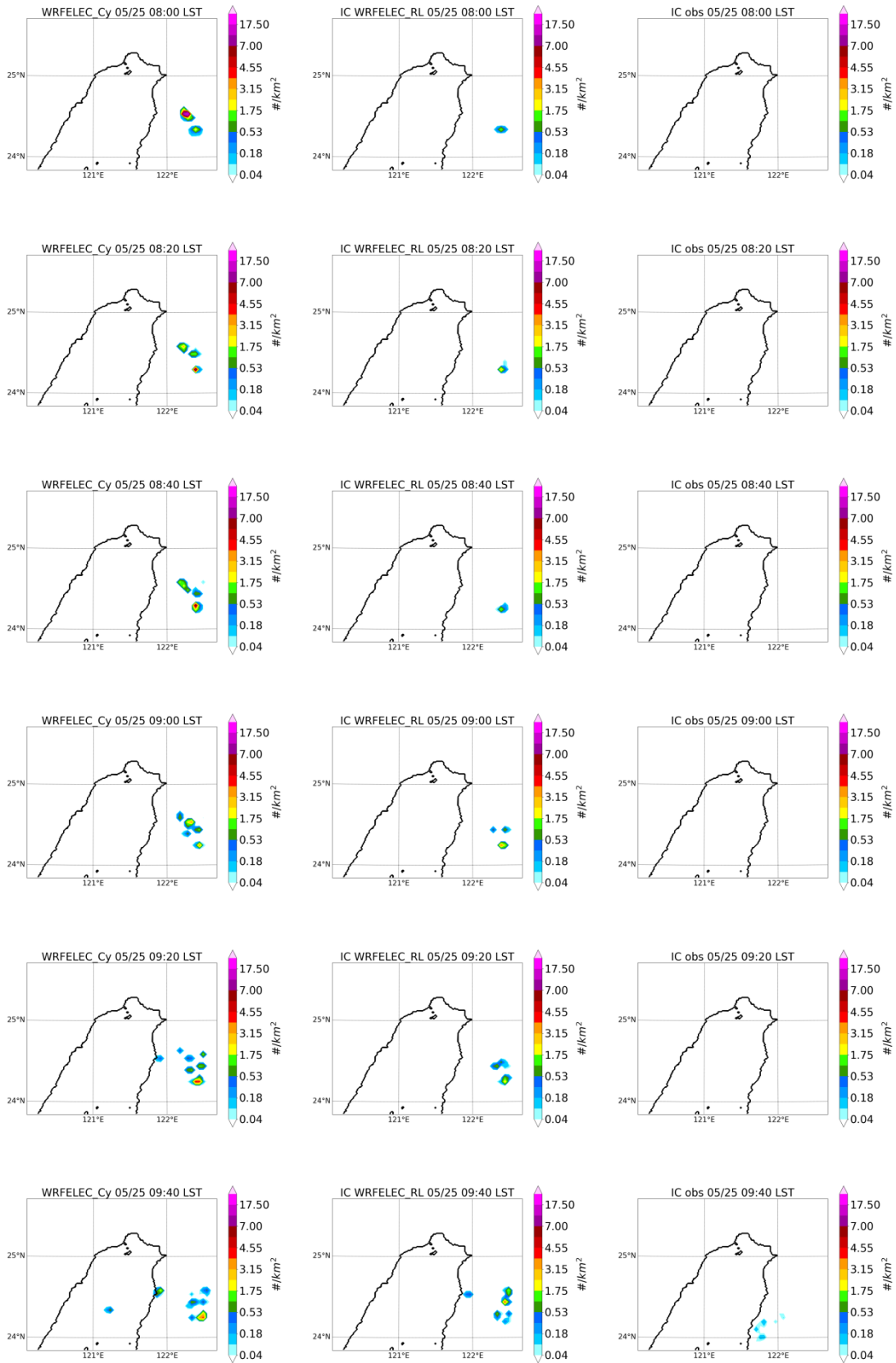
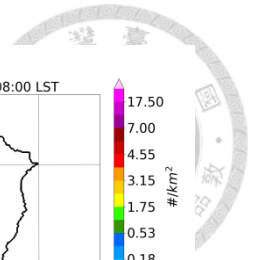
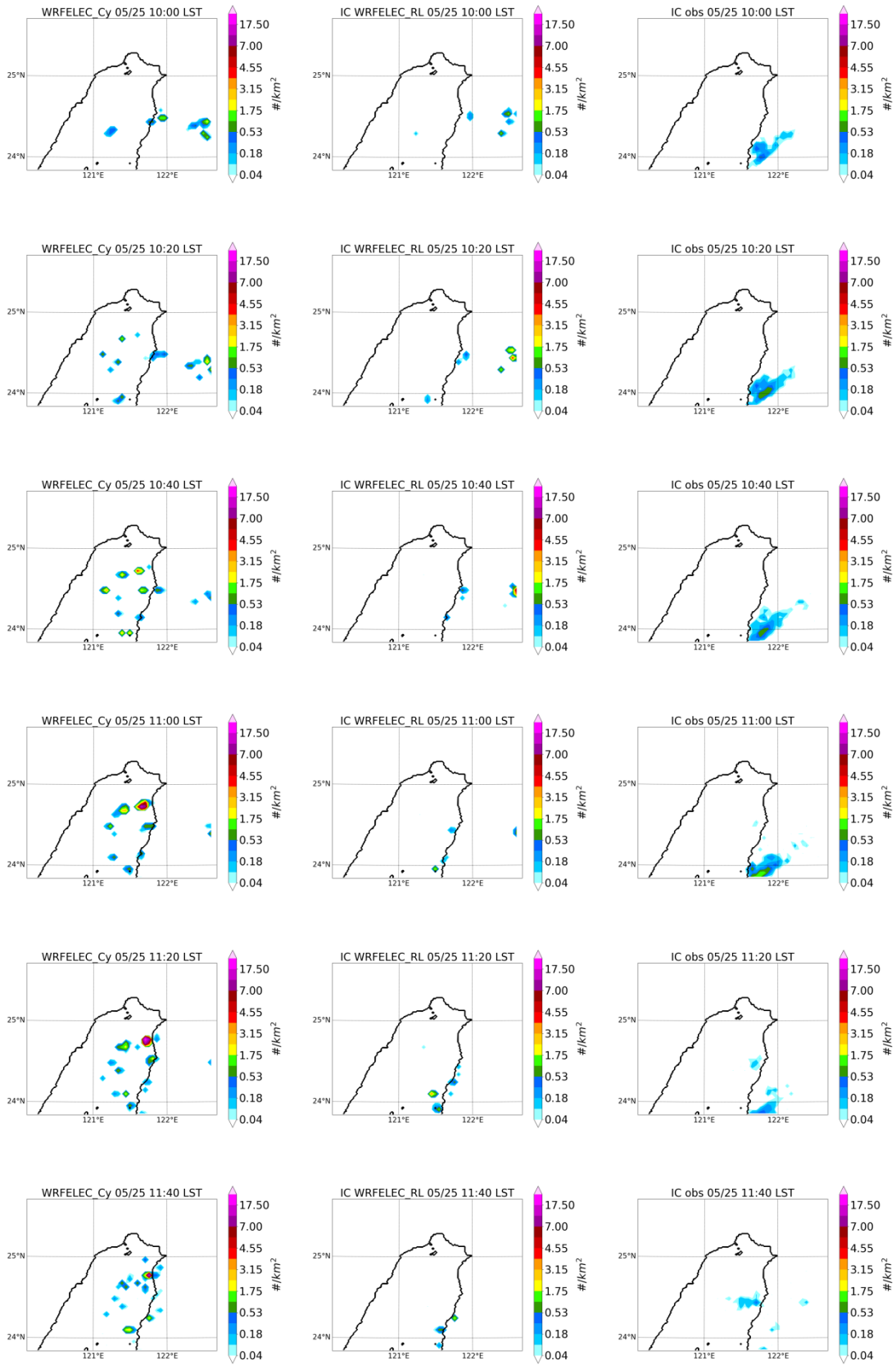
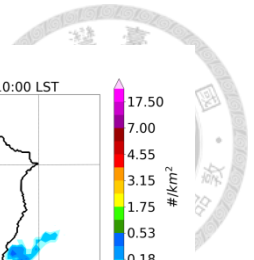


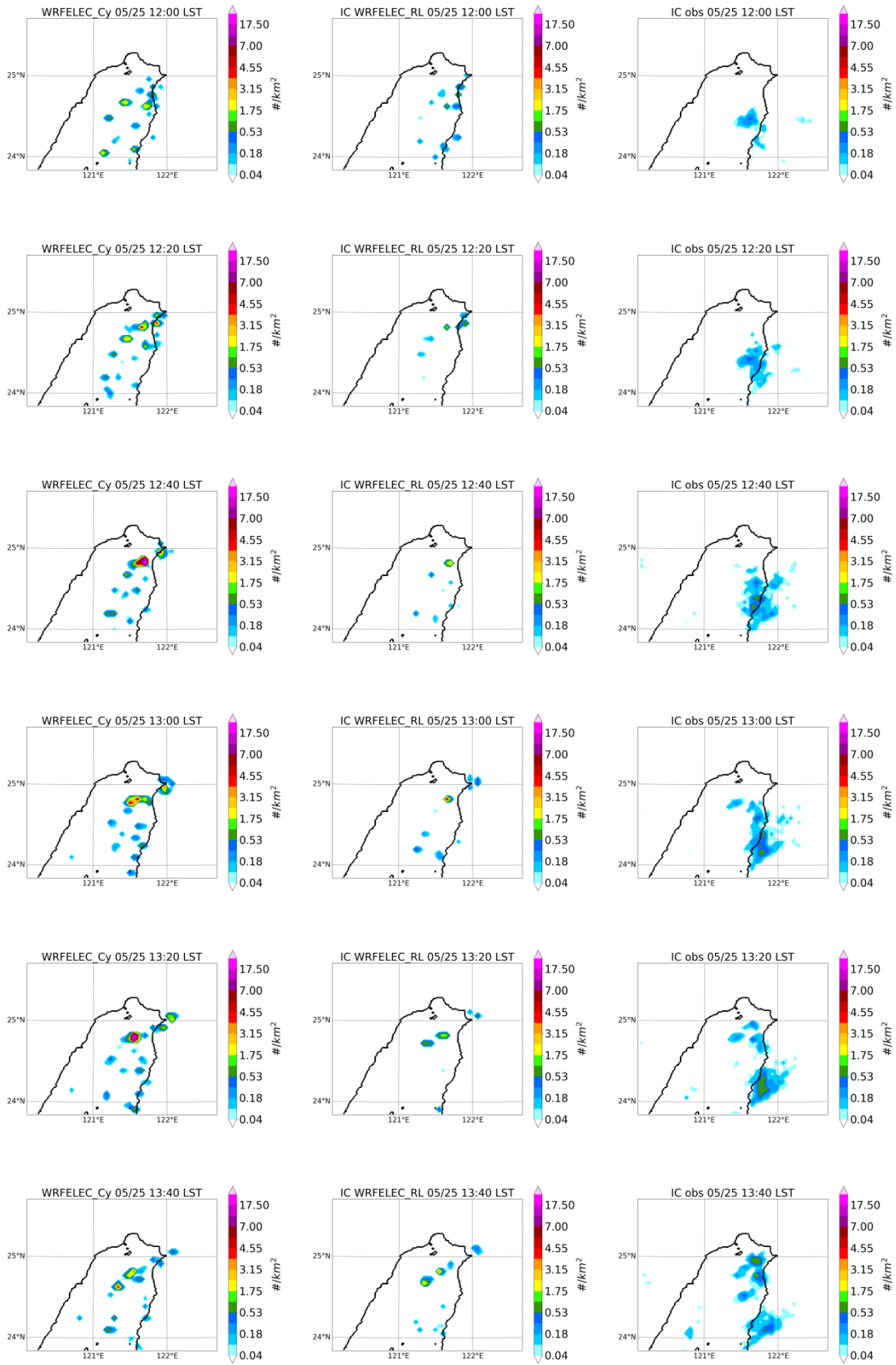
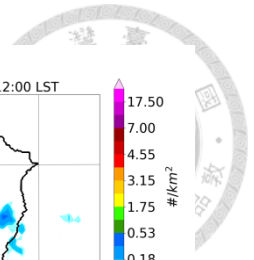
Figure A1: Composite reflectivity and three-dimensional view of convection cell. Left panel: simulated hydrometeors with mixing ratio of 0.5g/kg. Blue: graupel; Salmon: cloud drop; Green: rain drop; Red: cloud ice; Violet: snow; Brown: hail. Middle panel: simulated S-band (10cm) composite reflectivity. Right panel: composite reflectivity by the Central Weather Bureau radar system.

Appendix A2: Spatial distribution of Simulated and Observed Flashes.

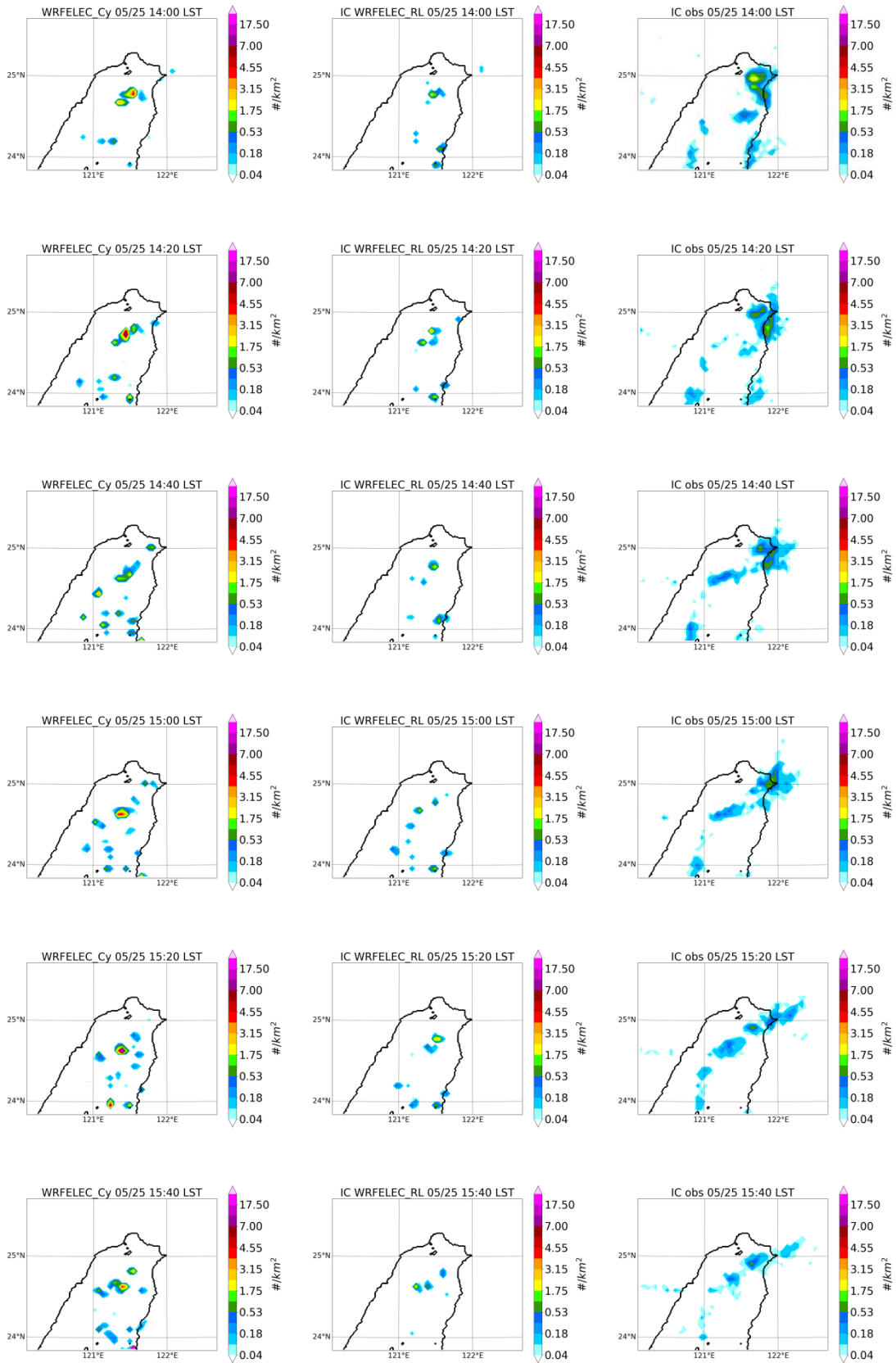
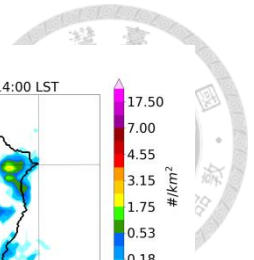


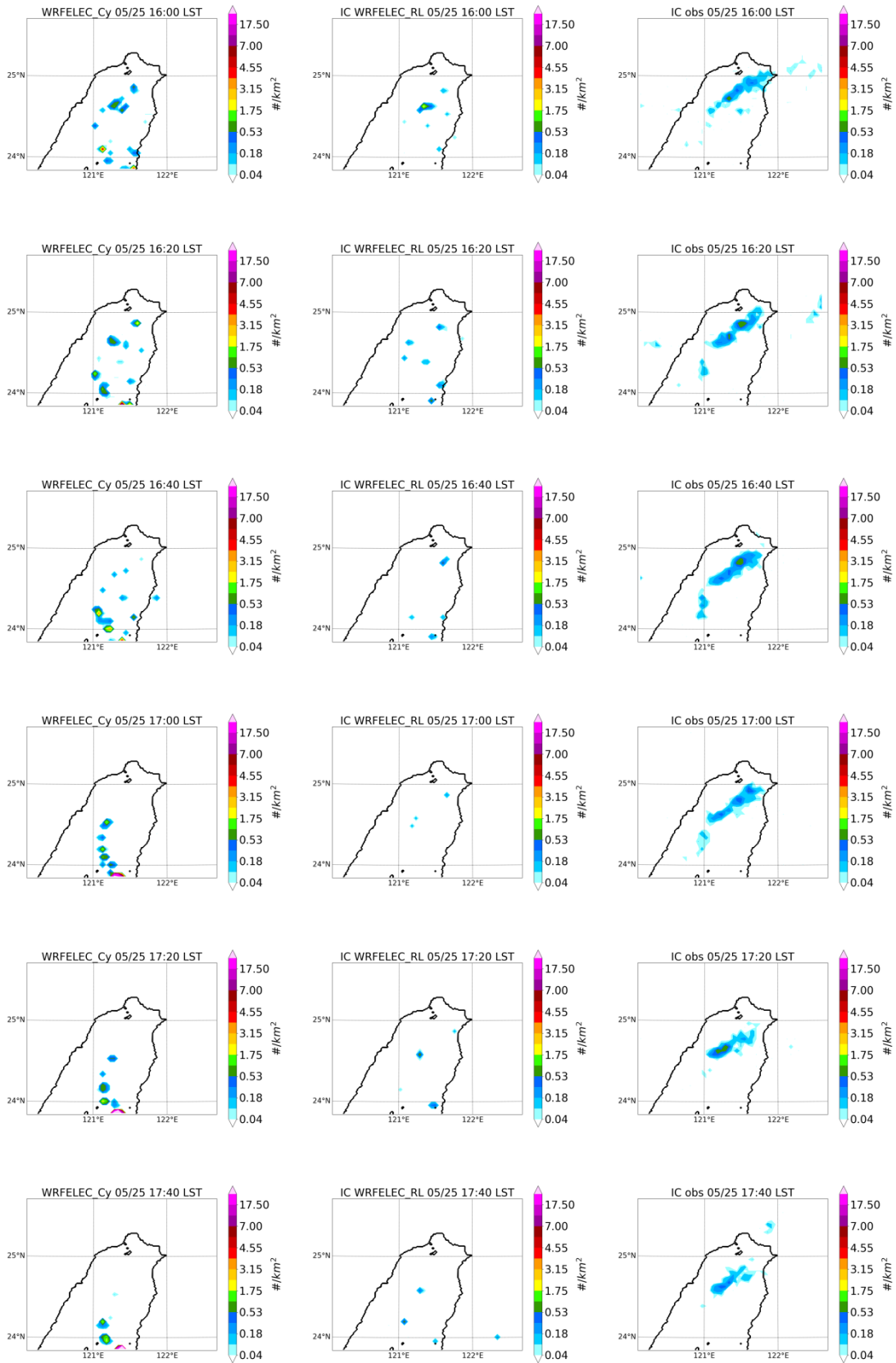
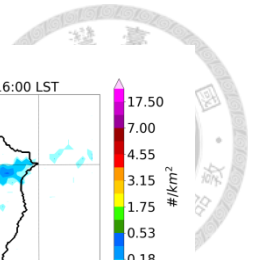


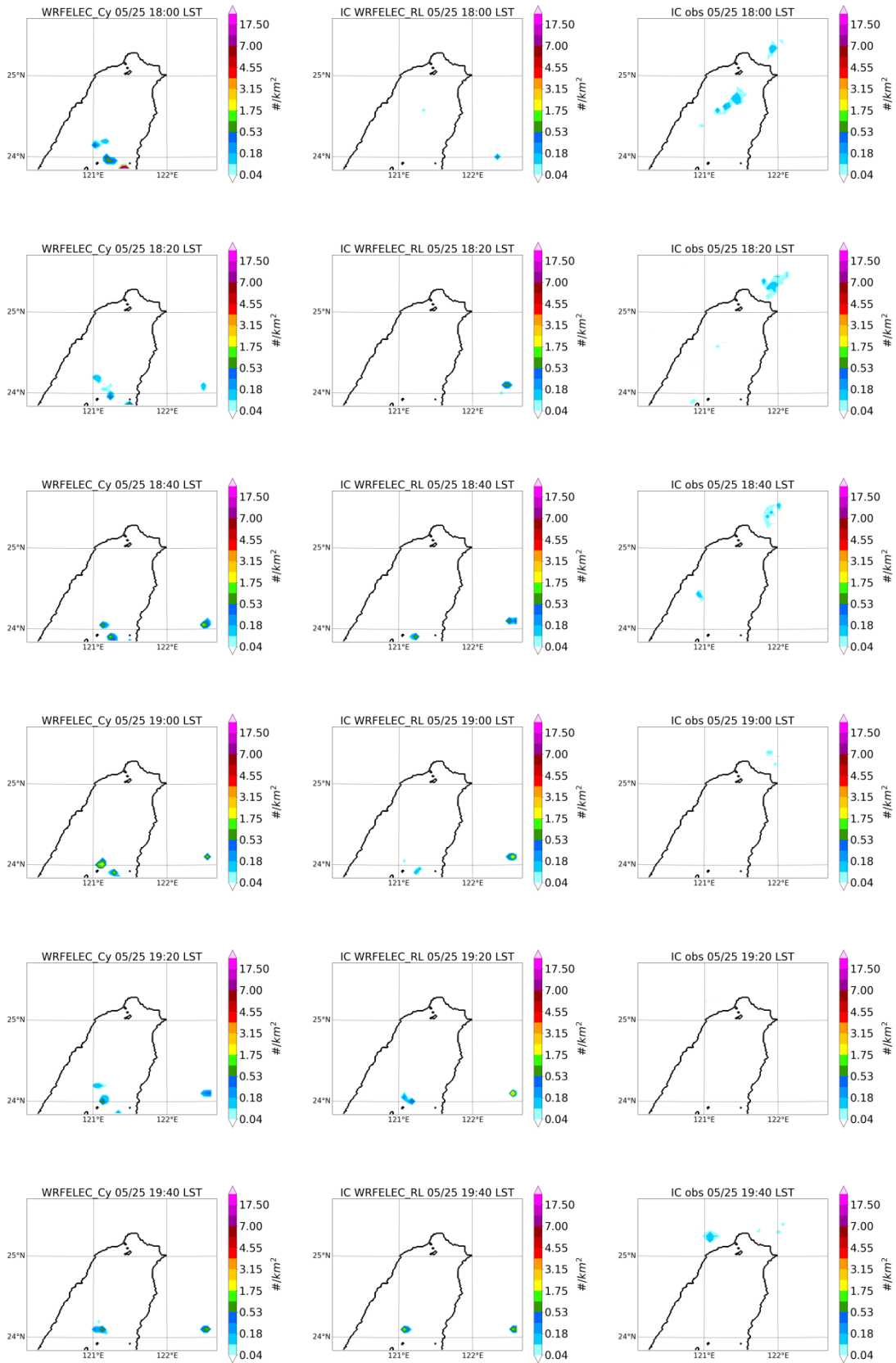
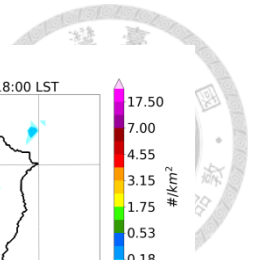












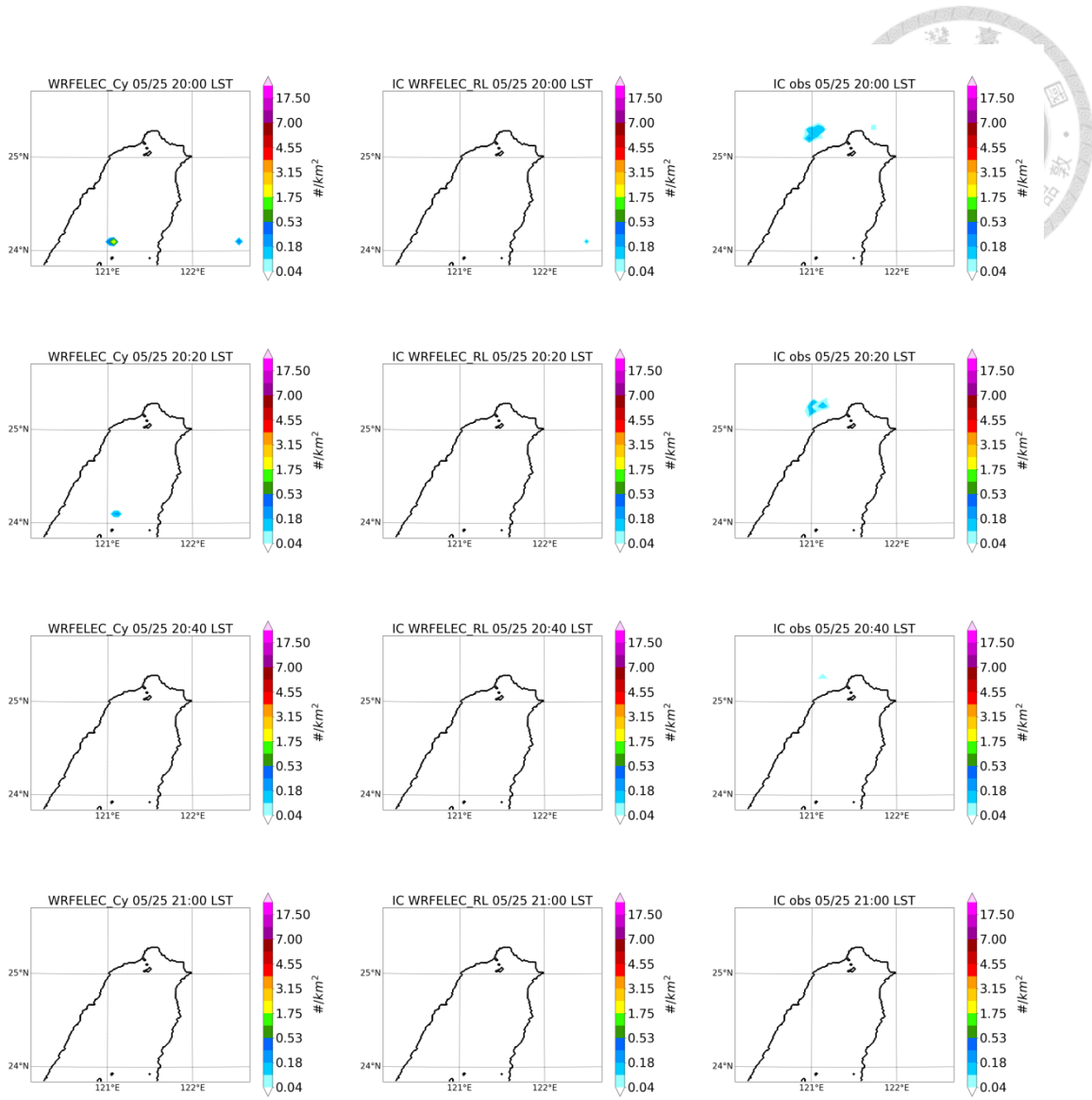
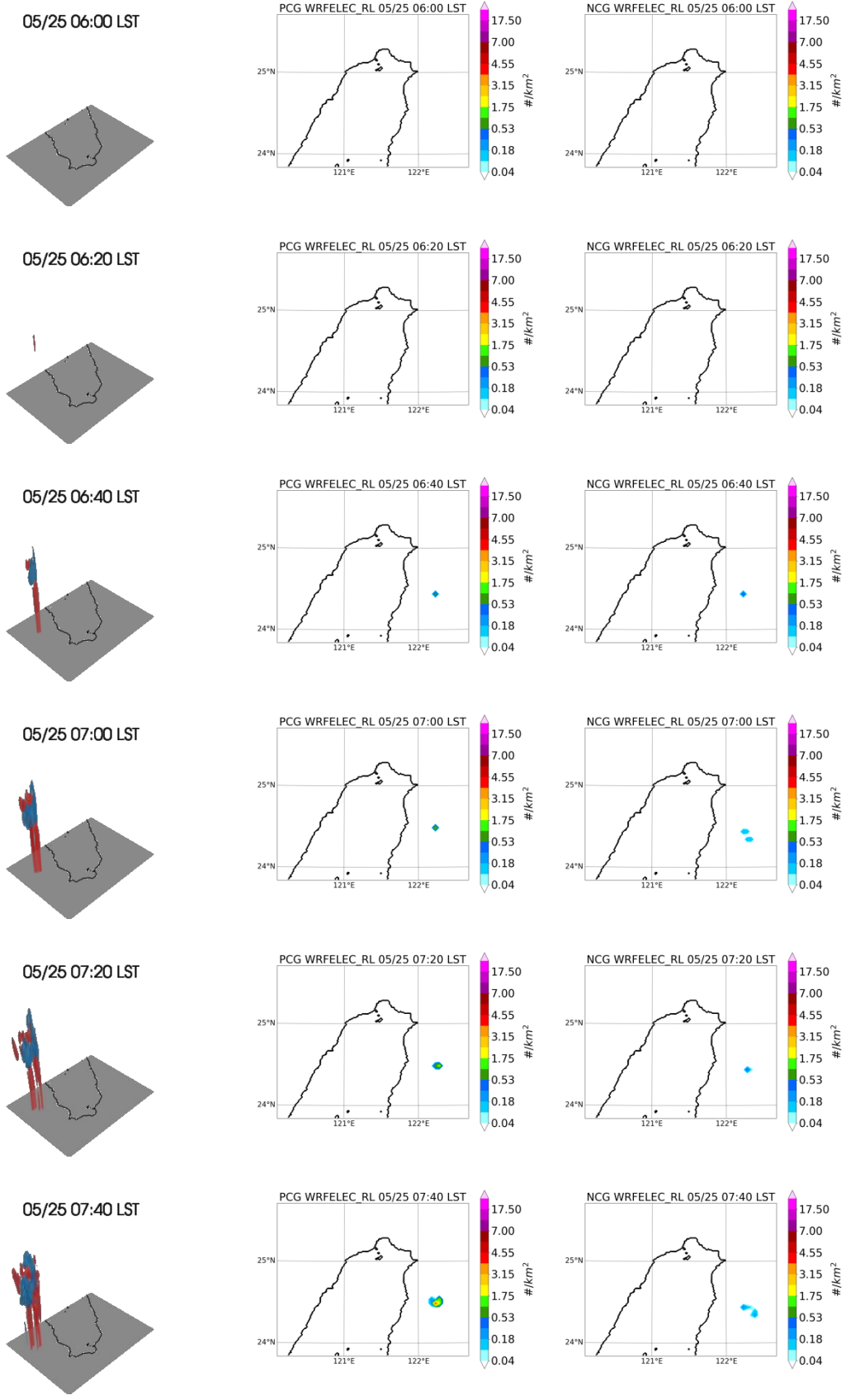
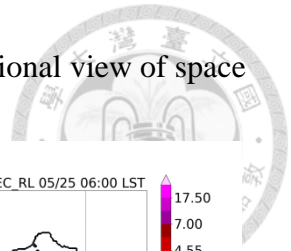
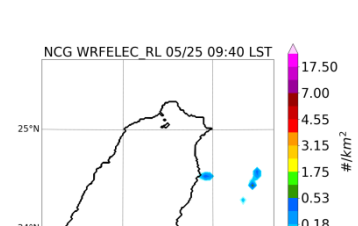
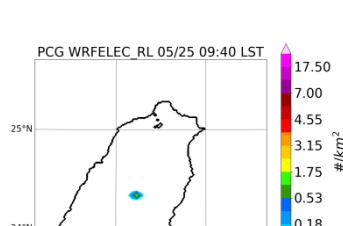
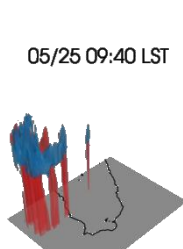
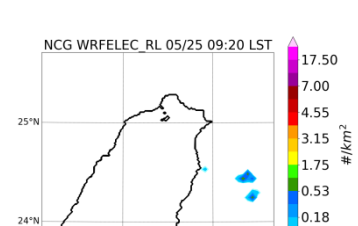
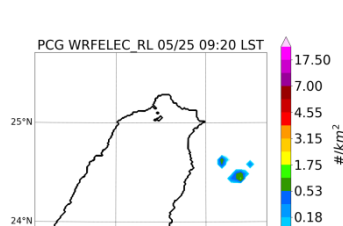
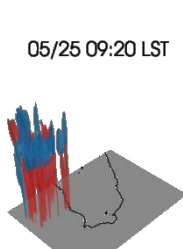
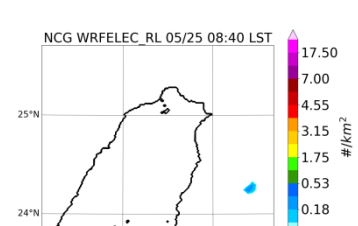
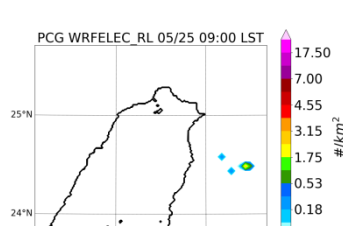
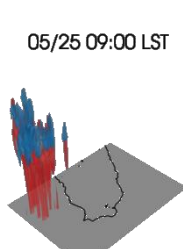
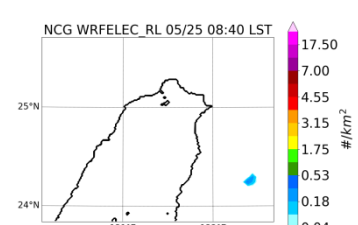
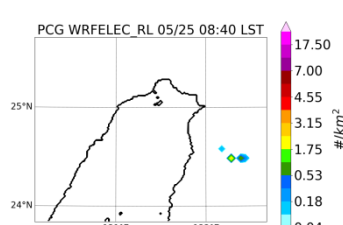
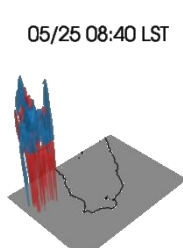
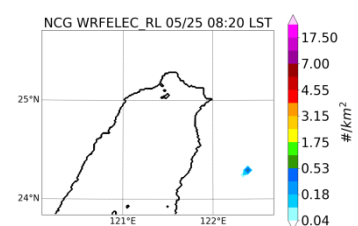
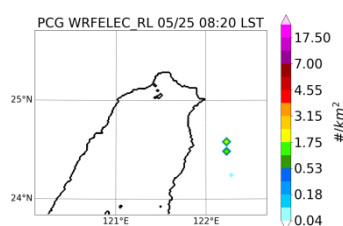
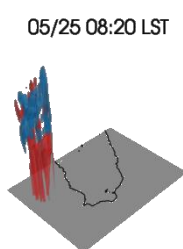
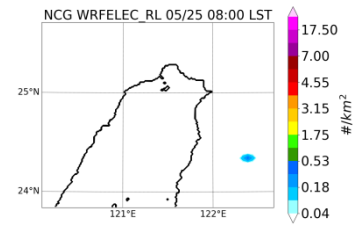
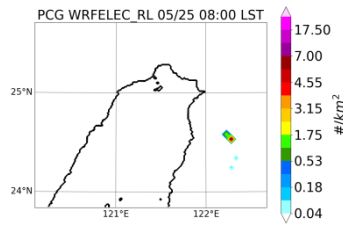
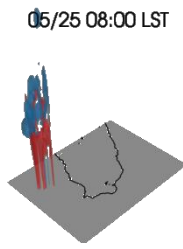
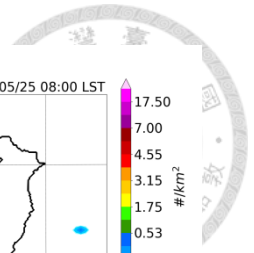
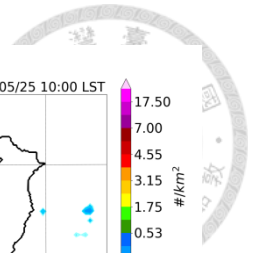


Figure A2: Spatial distribution of Flashes. Left panel: simulated flashes by Cy method. Middle panel: simulated IC by RL method; Right Panel: observed IC by TLDS.

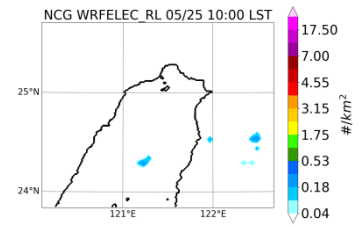
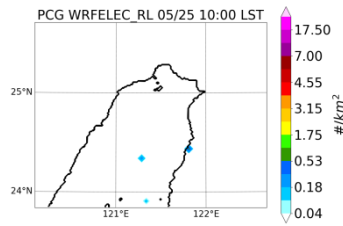
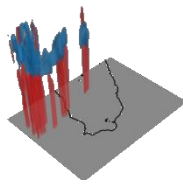
Appendix A3: Spatial distribution of simulated CG and three-dimensional view of space charges.



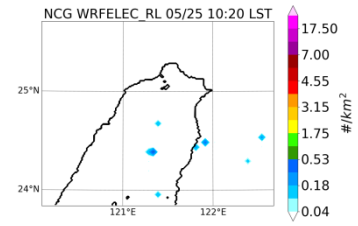
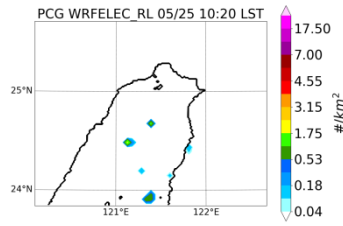
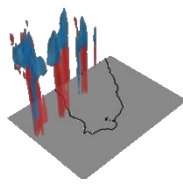




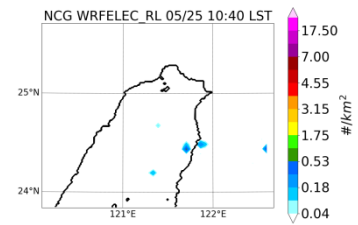
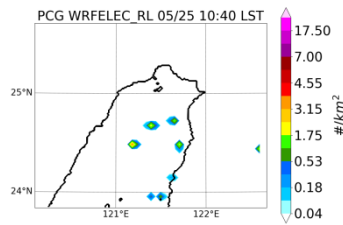
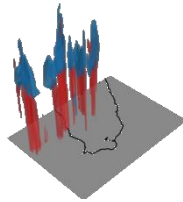
05/25 10:00 LST



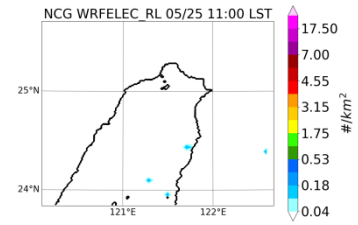
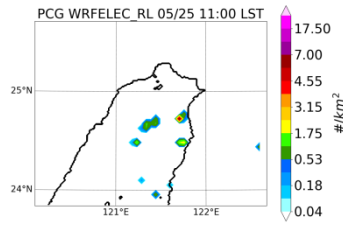
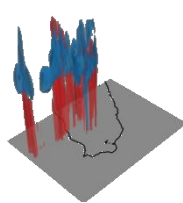
05/25 10:20 LST



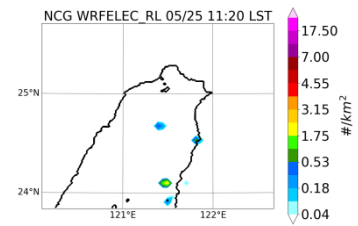
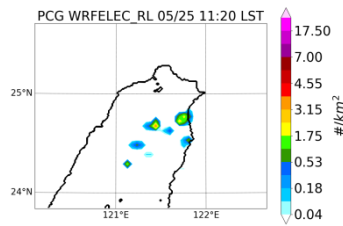
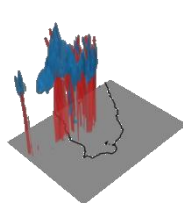
05/25 10:40 LST



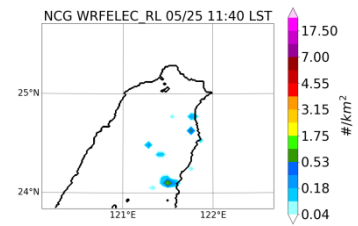
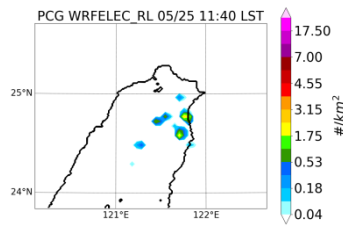
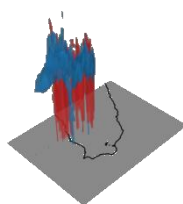
05/25 11:00 LST

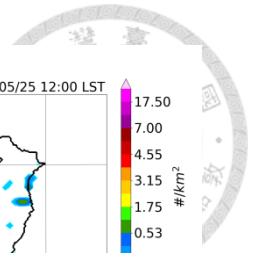


05/25 11:20 LST

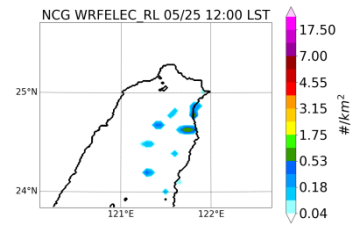
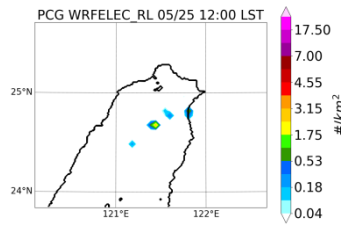
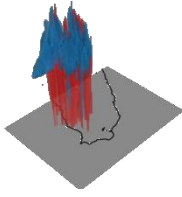


05/25 11:40 LST

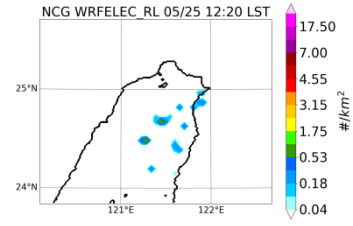
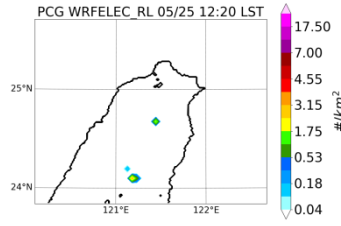
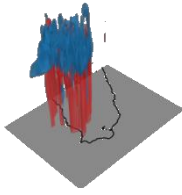




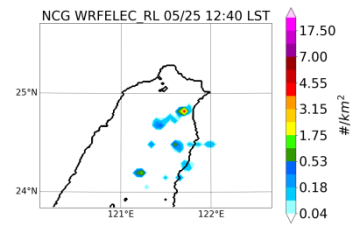
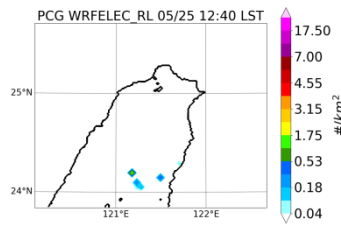
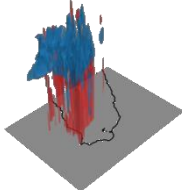
05/25 12:00 LST



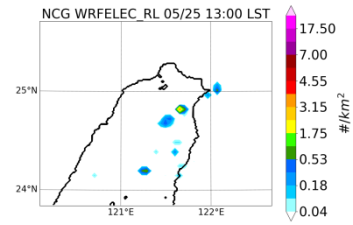
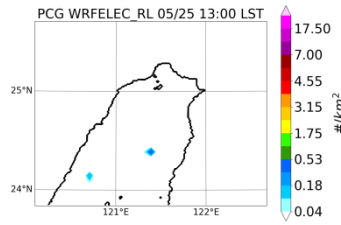
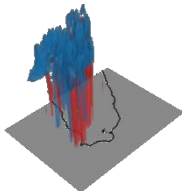
05/25 12:20 LST



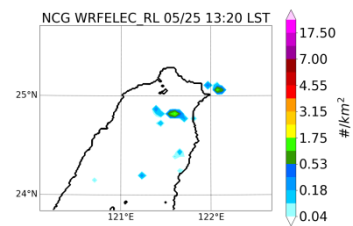
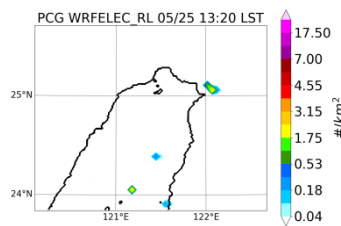
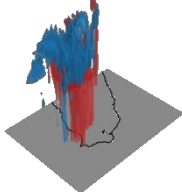
05/25 12:40 LST



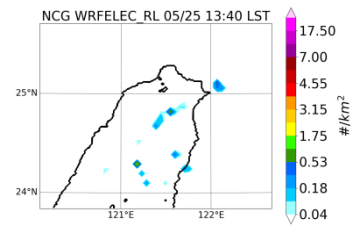
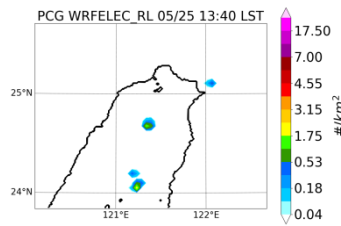
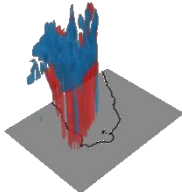
05/25 13:00 LST



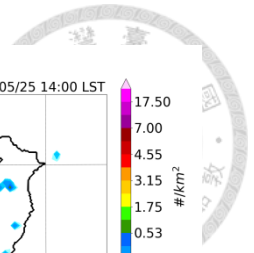
05/25 13:20 LST



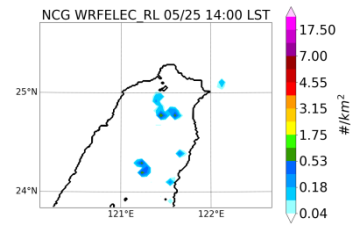
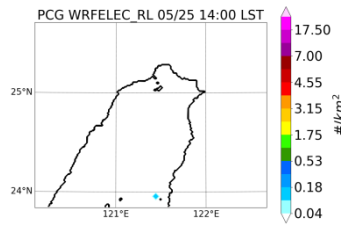
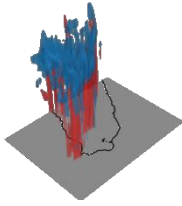
05/25 13:40 LST



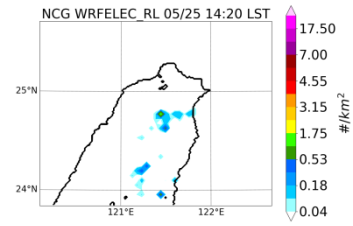
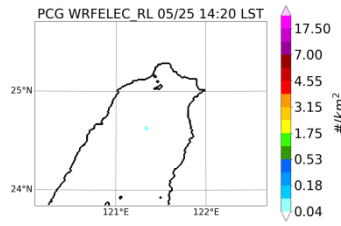
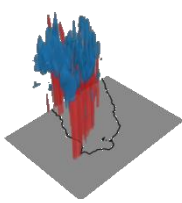




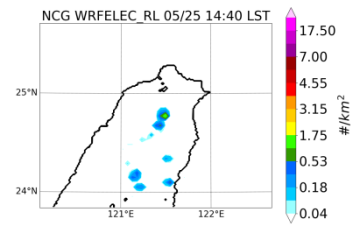
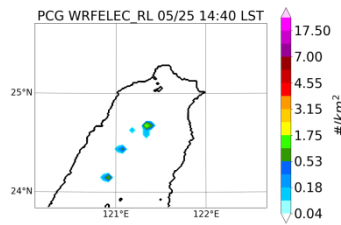
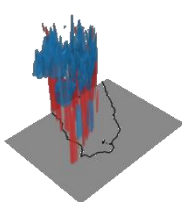
05/25 14:00 LST



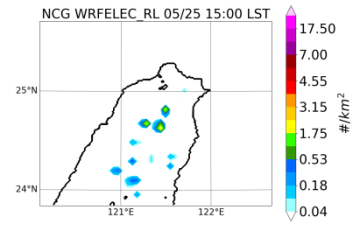
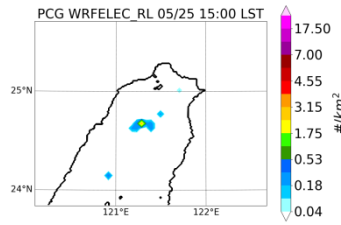
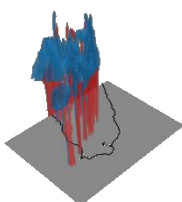
05/25 14:20 LST



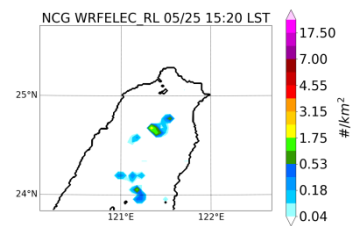
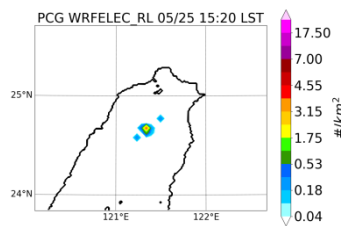
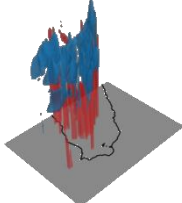
05/25 14:40 LST



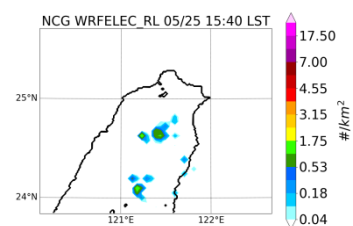
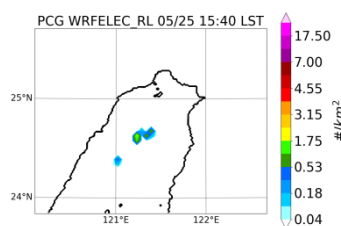
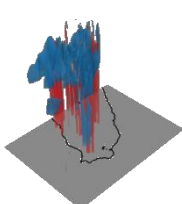
05/25 15:00 LST

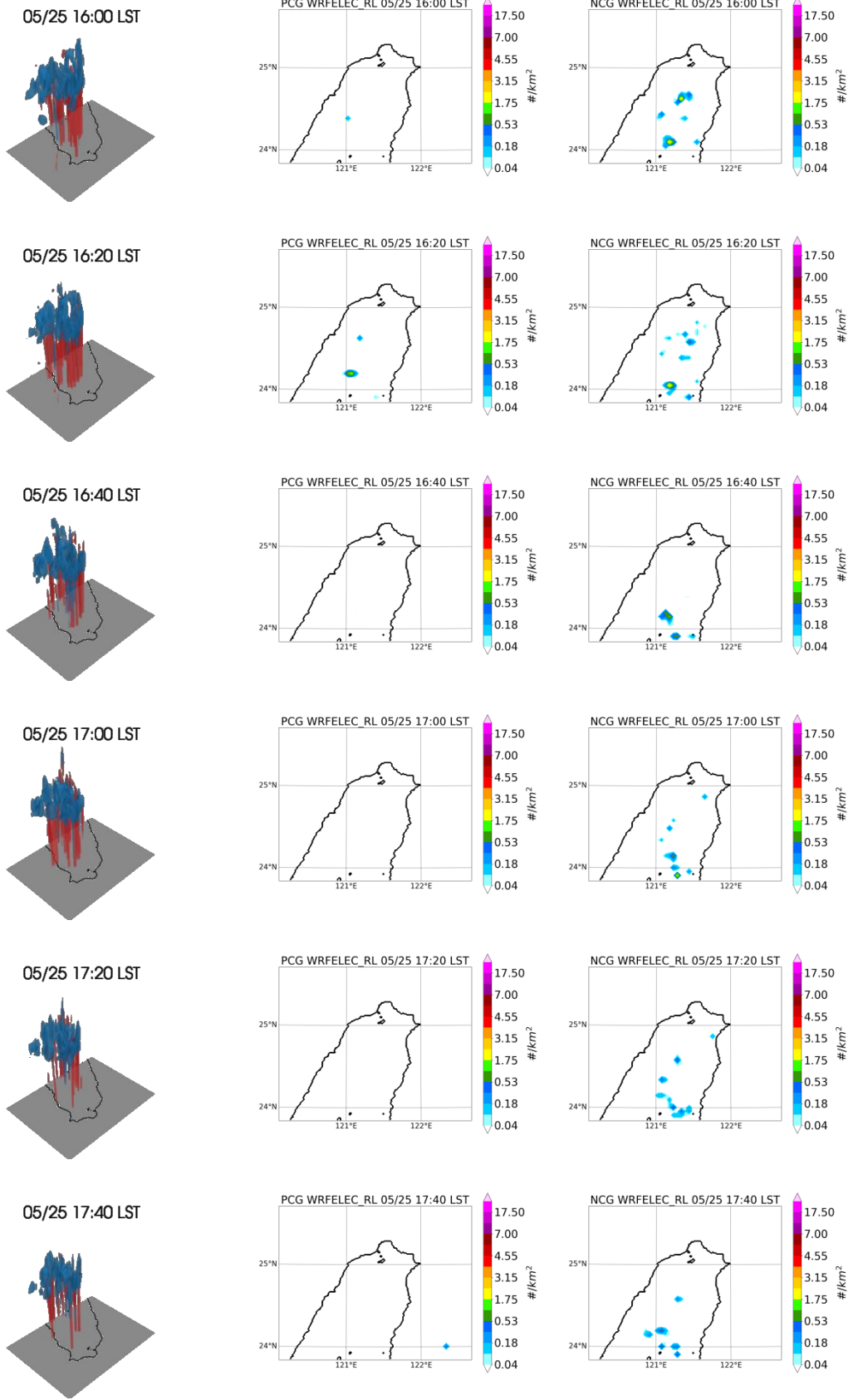
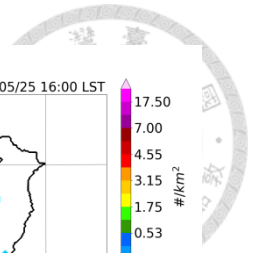


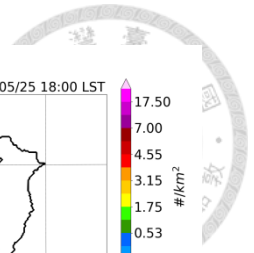
05/25 15:20 LST



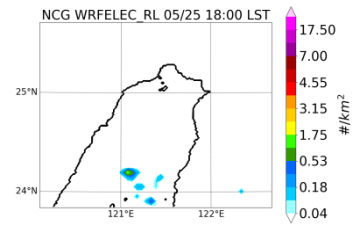
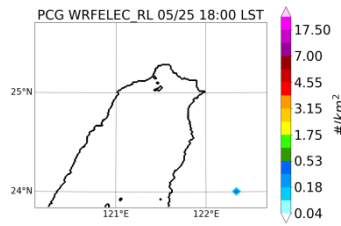
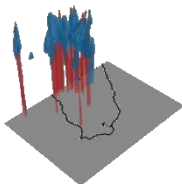
05/25 15:40 LST



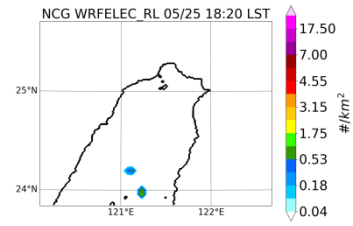
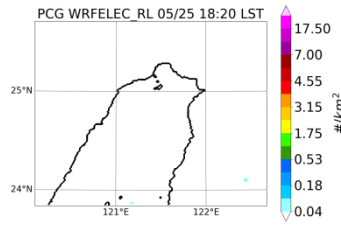
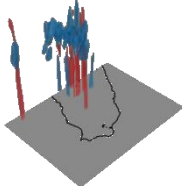




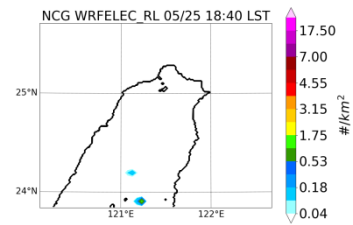
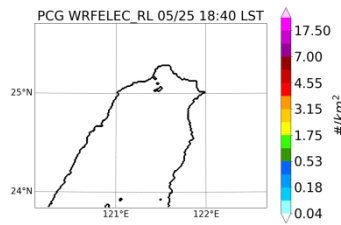
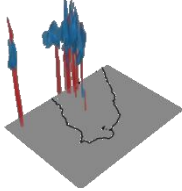
05/25 18:00 LST



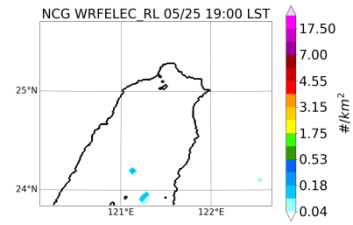
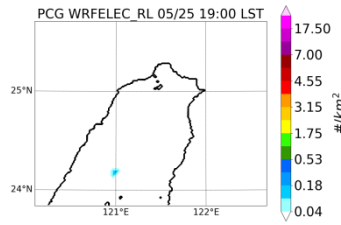
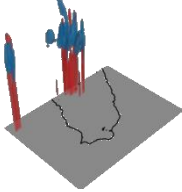
05/25 18:20 LST



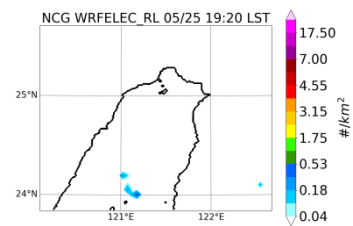
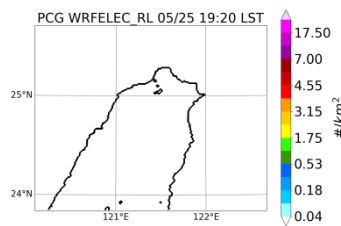
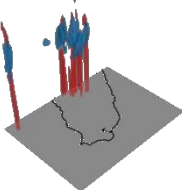
05/25 18:40 LST



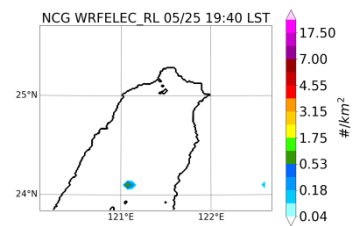
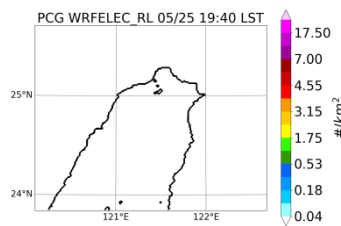
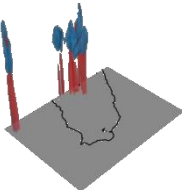
05/25 19:00 LST



05/25 19:20 LST



05/25 19:40 LST



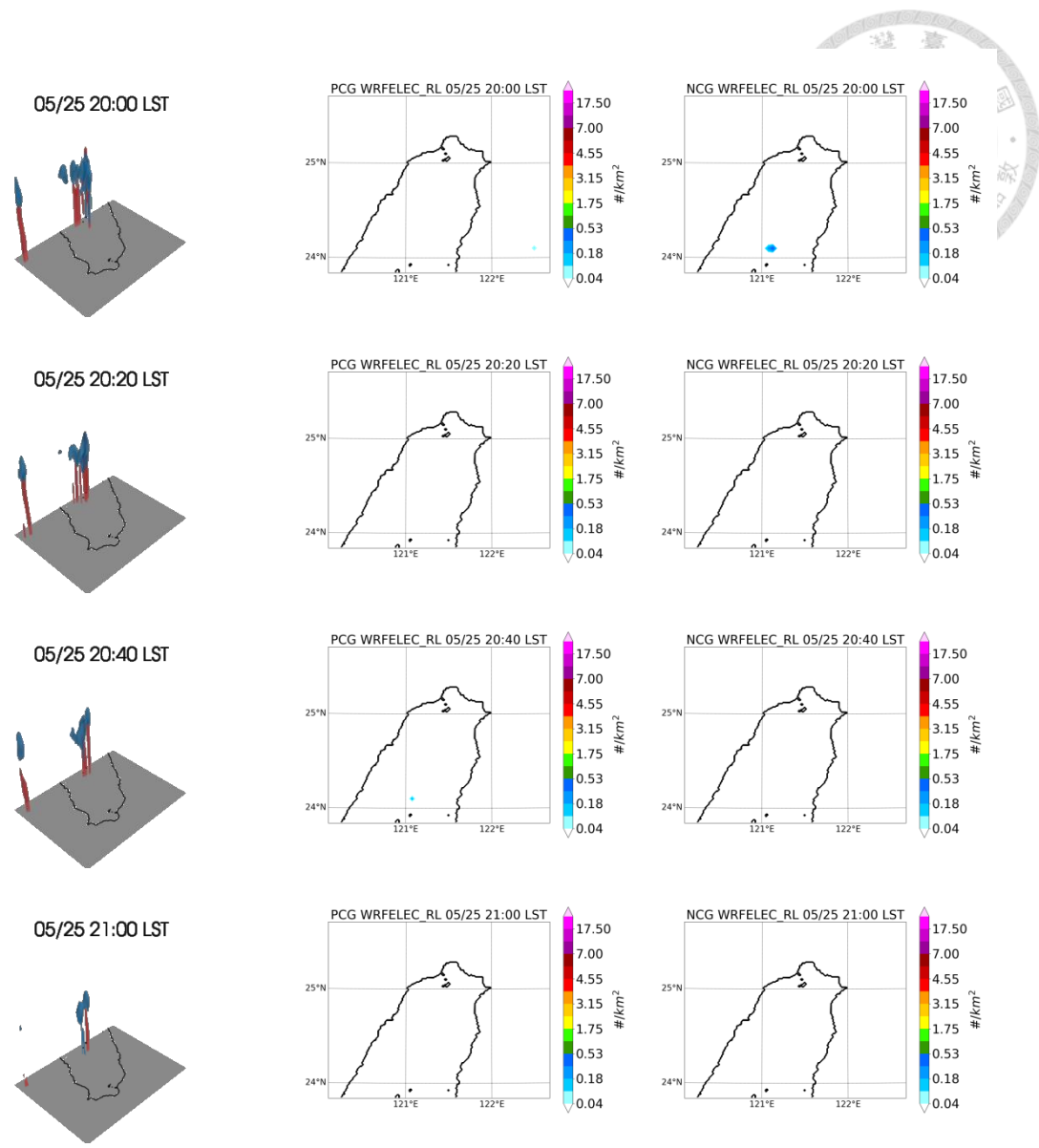


Figure A3: Spatial distribution of simulated CG and three-dimensional view of space charge. Left panel: simulated space charge with concentration of  $0.1\text{nC/m}^3$ . Blue: negative charges; Red: positive charges. Middle panel: simulated positive CG by RL method. Right panel: simulated negative CG by RL method.